Sonochemical Synthesis of alpha-Nickel Hydroxide from Urea and Hexamethyltetraamine and Electrochemical Characterization

by

Fatma Sinem Ertaş

A Thesis Submitted to the

Graduate School of Engineering

In Partial Fulfillment of the Requirements

The Degree of

Master Science

in

Material Science and Engineering

Koc University

September 2014

Koc University

Graduate School of Sciences and Engineering

This is to certify that I have examined this copy of a master's thesis by

Fatma Sinem Ertaş

and have found that it is complete and satisfactory in all respects,

and that any and all revisions required the final

examining committee have been made.

Committee Members:

Özgür Birer, Ph. D. (Advisor)

Oğuzhan Gürlü, Ph. D.

Funda Yağcı Acar, Ph.D.

Date: Sep, 12 2014

ABSTRACT

Sonochemical degradation of OH^- sources urea and hexamethyl tetramine were employed to synthesize alpha-nickel hydroxide from different nickel salts. Utilization of ultrasound yielded products with properties significantly different than the products obtained by thermal degradation of OH^- sources. The effect of intercalating chloride, nitrate, acetate, and sulfate anions on morphology and electrochemical performance was studied.

For the urea decomposition; the sulfate-intercalated sample had the smallest interlayer spacing when obtained by the sonochemical method, contradicting all the previous thermal synthesis results. The specific capacitance trend also differed from the literature values, and the value for the sulfate-intercalated sample was larger than that of acetate, chloride and nitrate intercalated samples. Ultrasonic synthesis increased the specific capacitance of the sulfate-intercalated sample significantly. This sample was also the most reversible and had the highest charge efficiency.

For the hexamethyl tetramine decomposition; electrochemical performance was increased with respect to urea decomposition since cyanate ion that is byproduct of the urea decomposition decrease the electrochemical performance. Specific capacitance of the nickel hydroxide was increased up to 50% for sulfate precursor. Alpha form of the nickel hydroxide was stable up to 300 cycle for each precursors. It was also examined that adding extra anion whether increase the electrochemical properties or not in this study. It was proved that adding extra anion increased the electrochemical performance 90% for sulfate precursor. It was also proved morphologically that adding extra anion made nickel hydroxide more crystalline.

ÖZET

Bu tezde üre ve heksametilen tetraminin sonokimyasal bozulmasıyla ortaya çıkan OH^- ve farklı nikel tuzları kullanılarak alfa-nikel hidroksit sentezlenmiştir. Ultrason kullanımı termal bozunması ile elde edilen ürünlere göre önemli ölçüde farklı özelliklere sahip ürünlerin elde edilmesini sağlanmıştır. Aynı zamanda klorür, nitrat, asetat, sülfat anyonları interkalasyonu ile nikel hidroksitlerin morfolojik ve elektrokimyasal performans üzerindeki etkisi incelenmiştir.

Üre kaynaklı sentez için; Eski çalışmalarda tüm termal sentez sonucu olarak sülfat -interkalar örnek için en küçük ara tabaka aralığı gözlemlenmekteyken, sonokimyasal olarak sentezlenen için en büyük ara tabaka aralığı gözlemlenmiştir. Ayrıca spesifik kapasitans eğilimi literatüre göre farklılık göstermektedir. Sülfat interkalar örneği asetat, klorür ve nitrat örneklerine göre daha yüksek spesifik kapasitans değerlerine sahiptir. Ultrasonik sentezi önemli ölçüde sülfat -interkalar numunesinin spesifik kapasitans değerini arttırdığı gözlemlenmiştir. Bu örnek aynı zamanda geri dönüşümün en iyi olduğu ve en çok yüksek şarj verimliliğine sahip olduğu kanıtlanmıştır.

Hekzametilen tetramin kaynaklı sentez için; üre ayrışma sentezinin yan ürünü olarak ortaya çıkan siyanat iyonu elektrokimyasal performansı azalttığı düşünüldüğünden OH kaynağı olarak hekzametilen tetramine kullanılırsa elektrokimyasal performansın artacağı düşünülmüştür. Nikel hidroksit için %50 oranında spesifik kapasitansın arttığı gözlemlenmiştir. Aynı zamanda nikel hidroksitin alfa formunu 300. syklik döngüsü kadar kararlı olduğu 300. döngüde yapısı bozulduğu incelenmiştir. Ayrıca, bu çalışmada elektrokimyasal performansı arttırmak için sentez sırasında ekstra anyon eklenmiş ve analizleri yapılmıştır. Ekstra anyonun sülfat kaynaklı sentezlenen nikel hidroksit için elektrokimyasal performansı % 90 arttırdığı kanıtlanmıştır. Ayrıca ekstra anyonun morfolojik yapıyı değiştirdiği ve hidroksitin daha kristalin yapıya geçtiği kanıtlanmıştır.

ACKNOWLEDGEMENTS

I am truly and deeply indebted to so many people that there is no way to acknowledge them all, or even any of them properly. Over the 7 years it has been my good fortune to encounter many people who have given me their time, companionship, patience, professional and personal help. I would like to thank my advisor, Dr. Özgür Birer for all his help through out my master thesis. He has given me opportunity to work in his group for 3 years including my last undergraduate semester. His guidance and criticism teach me not only how to evaluate a scientific work but also teach me how to encounter emotional changes in my personal life in most understandable way.

Perhaps the second best work I did in the this thesis was to choose an incredible committee: Dr. Oğuzhan Gürlül and Dr. Funda Yağcı Acar for accepting taking part in this special day for me.

I would like to thank Uğur Ünal for his endless and kindless during my all education.

I would like to express my gratitude to Dr. Annamaria Miko. She not only teach me how to analyze electrochemical data she has also given critical suggestions on my further studies. I am thankful to her for sharing her experience with me.

I would like to thank Eylül Saraç for her intelligence and deeply critical and analytical way of looking at ideas make her a fantastic colleague and home mate. She has valuable contribution to my studies. She was always there to help me in anyway. Willing to discuss both professional and personal problems with me and help me solve these problems with patience (not always patiently). I am really happy to such a good friend.

I thank Dr. Barış Yağcı for all the help and good advice. He was the master chief of SEM images and the "maklube" that has never been cooked for us. I am really happy to have both good teacher and such good friend.

I would like to appreciate special word of gratitude to my good friend and colleague Ece Aytan. More than anything, she is a fantastic witch friend. She was always there to make me feel good with her homemade medication. I am really lucky to have such a friend. This master would not finish without her even she is in America for her Ph.D degree. I am grateful that I have met her and have life long friend.

Family is extremely important to me in all likelihood because I am blessed to have such a wonderful one. I would like to thank my parents my father Rafet, my mother Arzu, my sisters Aslı and Kübra my sister's son Kuzey, my grandmother Suzan my grandfather Muzaffter for supporting me financially and morally during my studies. It is a pity my grandfather passed away in 2004 and did not see this day. They helped me in so many ways that there is no way I can repay them.

Without the love and support of my fiancée Sertaç I would be nowhere. It is his support that enabled me to go. It was his sacrifice to enable me to succeed. It is his love of life, joy, dance and kind-heartedness that is a daily reminder of why anyone does anything. I am so indebted to him there is no way to repay it. Thank you, my love , for everything.

Table of Contents

LIST OF TABLES

LIST OF FIGURES

NOMENCLATURE

AC	Alternative Current
IR	Infrared
SEM	Scanning Electron Microscope
XRD	X-ray Diffraction
CV	Cyclic voltammetry
SO_4^{2-}	Sulfate Anion
OH^-	HydroxideAnion
α-$Ni(OH)_2$	alpha-Nickel Hydroxide
β-$Ni(OH)_2$	beta-Nickel Hydroxide
NiOOH	Nickel Oxihydroxide
Cl^-	Chloride
NO_3^-	Nitrate
SCN^-	Cyanate
$Ni(OH)_2$	Nickel Hydroxide
KOH	Potassium Hydroxide
HMT	Hexamethylene Tetramine
$CO(NH_2)_2$	Urea
NH_2	Amine
wt.%	weight percent
GC	Galvanostatic Charge-discharge
I	Current

Chapter 1

1. Introduction

1.1. Introduction to Sonochemistry

Sonochemistry is the area that studies the effect of sonic waves and wave properties on the chemical systems. The frequency range from 20 kHz to -1 MHz is generally used in sonochemistry. The number of the papers published in sonochemical processes increased dramatically in the last 30 years since the commercial and cheap devices were produced.

Sound is transmitted in an elastic medium as a longitudinal wave. This transmission causes compression and expansion cycles in medium. During this expansion and compression, the positions of molecules changes so distance between them changes. If the medium is liquid, the liquid molecules are forced with ultrasonic waves and pressure on the molecules. As the expansion, called the negative pressure, becomes large enough, molecules which are held together with intra-molecular interaction can be separated forming the acoustic cavitations. These cavities in a fluid produced by ultrasound are highly energetic. After bubbles (cavities) are generated the ultrasound oscillates cavitations at the size of the source frequency. Typical size of a bubble is about1-5 μm. [1] During this step bubbles in liquid medium grows and after a certain point it collapses. It is called the transfer of the energy from macro scale (acoustic wave) to micro scale (bubble in liquid). During this transfer of the energy unique environment, localized high temperature and high pressure conditions are generated in micro scale. [2] Highly reactive free radicals are generated at this condition. These radicals enhance chemical processing.

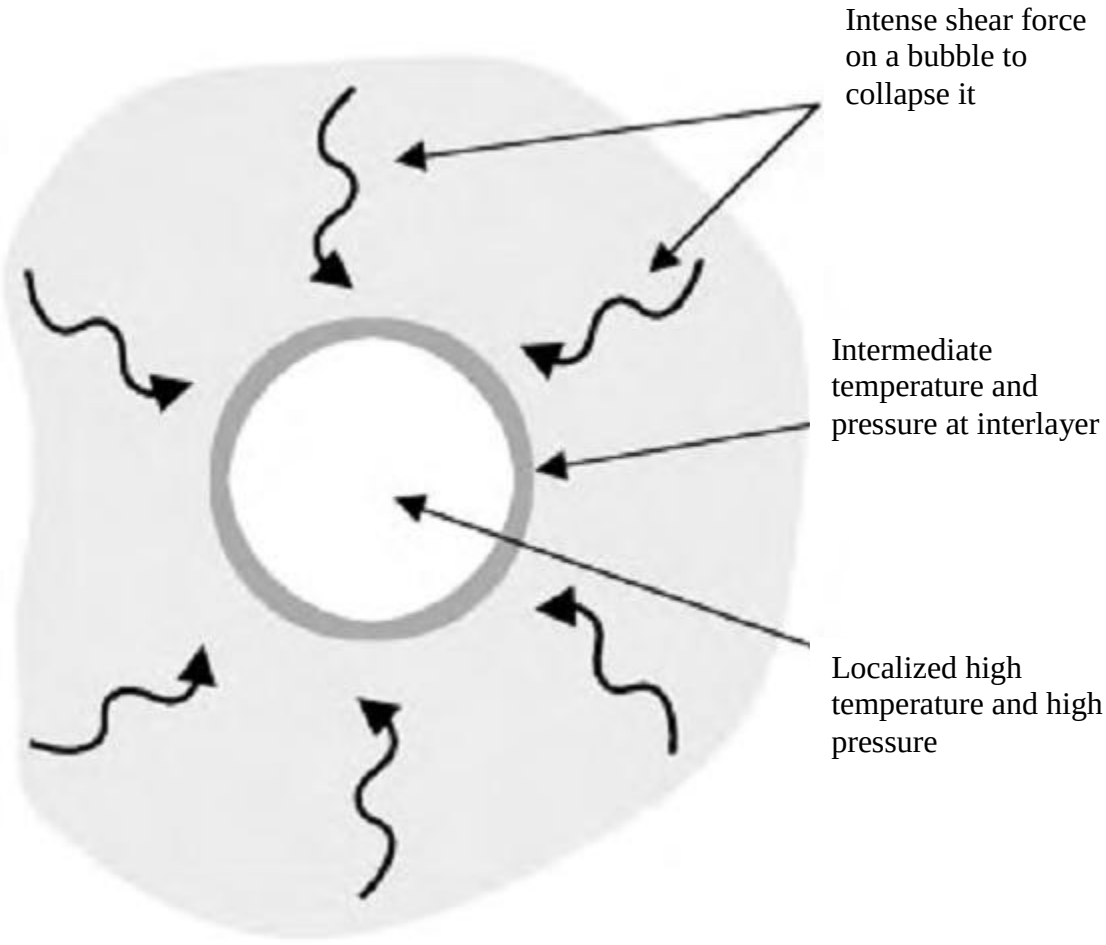

Figure 1 Representation of temperature and pressure in a liquid medium with the effect of sonication.

Cavitations are associated with the formation, growth, and collapse of bubbles in a liquid. During the forming and then collapsing the cavitations pressure fluctuations were generated by ultrasound waves in a liquid medium. The localized temperature in sonicated system was measured around 5200 K by using the reaction rate and Arrhenius equation by Suslick' group [3]. It is called as hot spot theory.

In liquid system, viscosity, surface tension and the vapor pressure of the liquids affect the cavity. Temperature is also one of the important parameter that affects the cavity frequency since vapor pressure of the liquid is directly related with the temperature. Reaction temperature affects the cavities. Increase in the reaction temperature lowers the intensity of the acoustic cavitations. In other words, to get the maximum effective sonochemical benefit lower temperature should be applied on to the system. [1]

As mention above during sonochemical reaction some radicals are produced. Hydroxyl radical ($HO^{\bullet}$) is formed in a sonochemical system containing water as solvent but solvent decomposition is normally minor contribution in sonochemical reaction taking place in the medium. All off below reactions are possible in the presence of water in sonochemical system:

$$H_2O \longrightarrow HO^{\bullet} + H^{\bullet} \quad (1)$$

$$HO^{\bullet} + HO^{\bullet} \longrightarrow H_2O_2 \quad (2)$$

$$HO^{\bullet} + HO^{\bullet} \longrightarrow H_2O + \tfrac{1}{2} O \quad (3)$$

$$HO^{\bullet} + HO^{\bullet} \longrightarrow H_2 + O_2 \quad (4)$$

$$H^{\bullet} + O_2 \longrightarrow HO_2^{\bullet} \quad (5)$$

$$HO_2^{\bullet} + H^{\bullet} \longrightarrow H_2O_2 \quad (6)$$

$$HO_2^{\bullet} + HO_2^{\bullet} \longrightarrow H_2O_2 + O_2 \quad (7)$$

$$HO^{\bullet} + HO_2 \longrightarrow H_2O_2 + O^{\bullet} \quad (8)$$

$$HO^{\bullet} + H^{\bullet} \longrightarrow H_2O \quad (9)$$

Other parameters which are important for the formation of cavitations are gas in the solution and the amplitude of the sonic waves. Gas in the system helps for the formation of cavitations by acting as nucleation site for the cavitations nucleation. During the reaction gas may come out but they are removed from the reaction mixture in time. Bubbling gas through the reaction solution increases the cavitations formation. The intensity of ultrasound is another requirement in order to form critical cavitations in the solution. The

intensity of the ultrasound is proportional to the square amplitude of the sonic wave. Increase in intensity of the amplitude increases the cavitations formation. [4]

Ultrasonic baths and horns are used for the generation of the ultrasound for the liquid systems. A piezoelectric material by applying high AC voltage produces ultrasound waves. For ultrasonic baths intensity of the ultrasound waves are quite low so ultrasonic horns are used to generate intense source of ultrasound for sonochemical systems.

The ultrasonic horns are made from titanium and it alloys. These metal tips may be affected from the ultrasound. Cavitations may erode surface as seen below [1]:

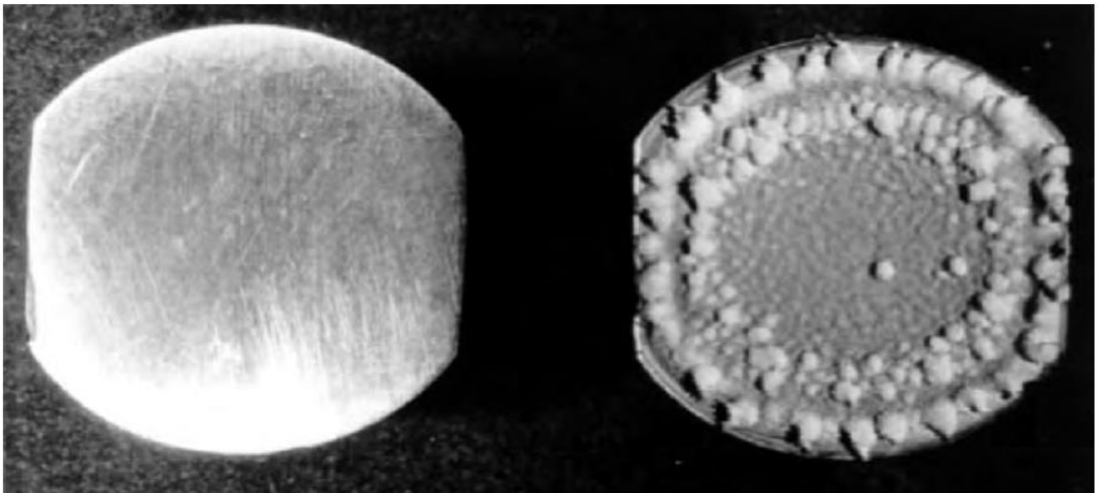

(a) **(b)**

Figure 2 (a) titanium alloy tip initial surface; (b) eroded surface

A typical setup for the horn system is given in Figure 3 [5].

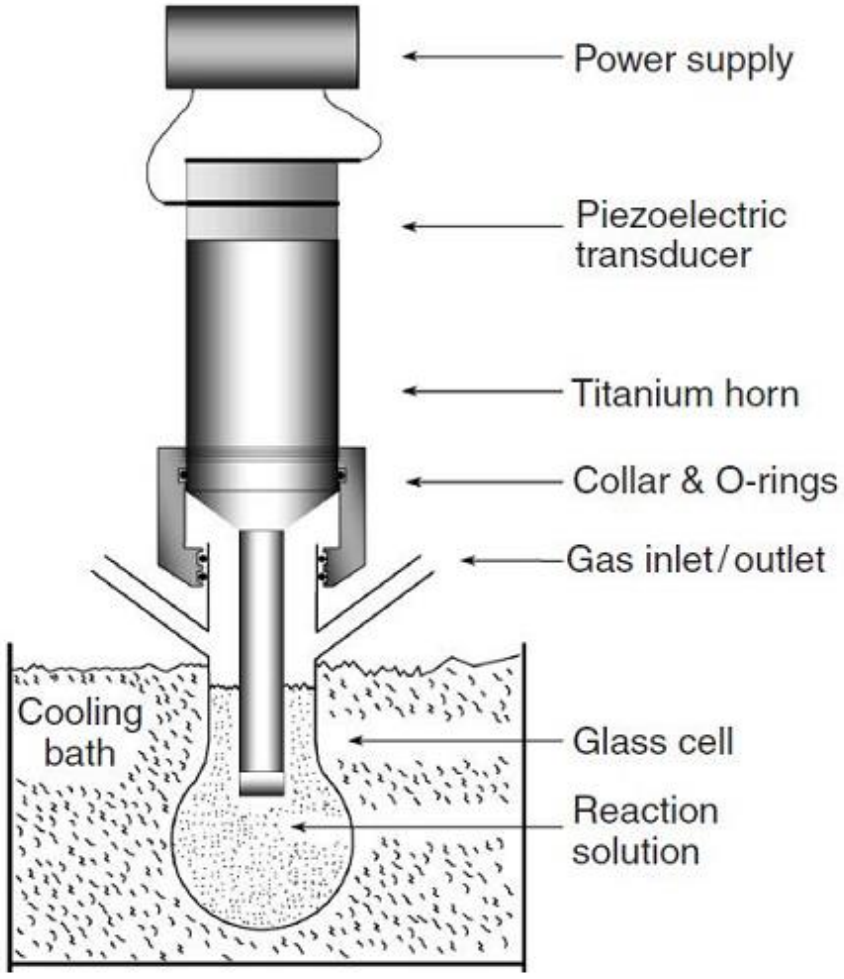

Figure 3 Experimental setup for sonochemical reaction

1.2. Application to Material Chemistry

Sonochemistry has wide range application. Some examples of these ultrasonic processes are ultrasonic cleaning, wet chemistry, electroplating, and production of foams and aerosols. [6] Morphology and size are other properties that make sonochemistry attractive and fundamental interest. [7,8,9] Shape control methods with the sonochemistry utilize the differences in shape of the material instead of using surfactant. [7]

1.2.1. Metal Oxide / Hydroxide

Metal oxides and metal hydroxide are used as energy storage materials for capacitors. In recent years, oxide/hydroxide electrodes have been studied extensively in the literature since it has been prompted by the uses these materials found in energy storage technology. For instance, transition metal oxides based on nickel [10,11,12], cobalt [13], manganese [14] , and iron [15] have been identified as possible electrode materials for electro-chemical supercapacitors, whereas $Ni(OH)_2$ is widely used as a cathode material in Ni–Cd and Ni–Metal hydride batteries[16,17].

1.2.2. Nickel Hydroxide

Nickel hydroxide exists in four different forms which consist of α-$Ni(OH)_2$, β-$Ni(OH)_2$, γ-NiOOH and β-NiOOH. The first two are the most common forms of nickel hydroxide and crystallize in a hexagonal system while the latter two are the oxyhydroxide forms of α-$Ni(OH)_2$ and β-$Ni(OH)_2$. α-$Ni(OH)_2$ form has more disordered and larger interlayer spacing (7-8 Å) as the interlamellar space contains anions such as nitrate, carbonate, sulfate, chloride, or water molecules.

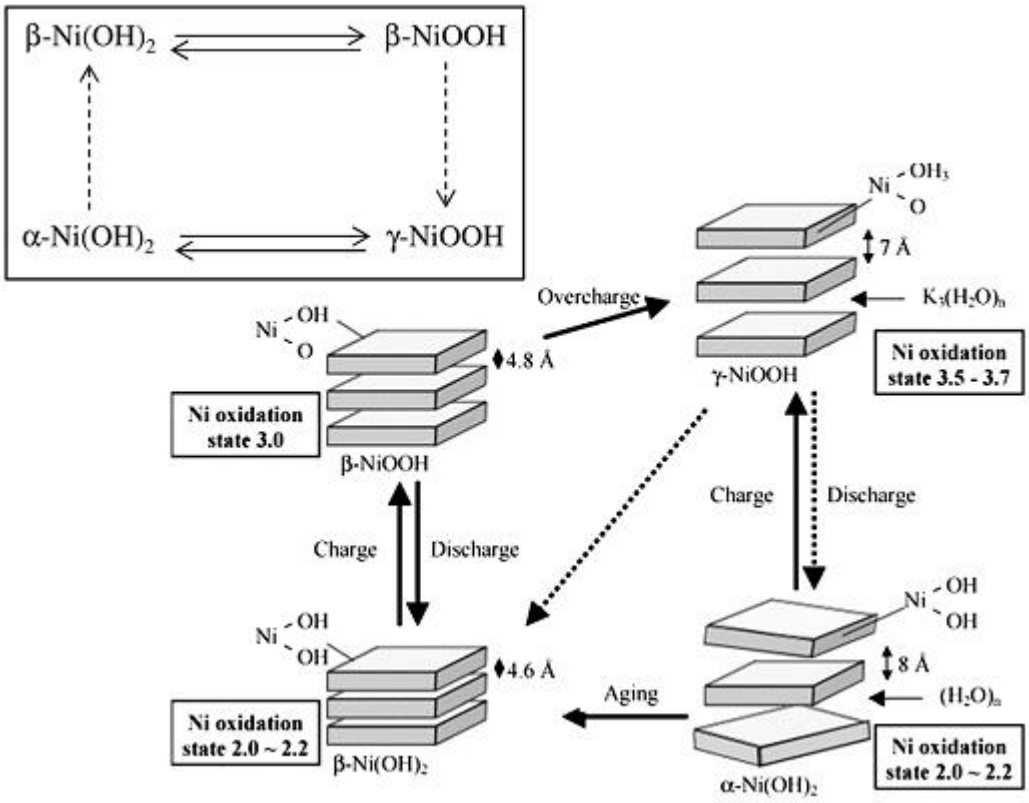

Figure 4 Schematic representation of the Bode cycle for the Ni(II)/Ni(III) redox transition in Ni hydroxide layer. [18]

Electrode half-cell reaction is represented as:

$$Ni(OH)_2 + OH^- \longrightarrow NiOOH + H_2O + e^- \qquad (10)$$

1.2.3. Electrochemical Properties of Nickel Hydroxides

Nickel hydroxide is an important functional material used in nickel batteries, catalysts, electrochromic devices, and ionic exchangers. The stability problem of α form is transformation into β in its strongly alkaline electrolyte (generally 6 M KOH) during cycling or storage. [19] The α-$Ni(OH)_2$ is not currently used in battery applications because its charge capacity tends to decrease more rapidly on cycling than that of β-$Ni(OH)_2$

electrodes. [20] The β-$Ni(OH)_2$ phase is brucite-like and well-oriented. $Ni(OH)_2$ layers are perfectly stacked along the c-axis with an intermaller distance of 4.6 Å. The beta form has higher stability in alkaline solutions but it has lower theoretical specific capacity of 289 mAh/g (1072 F/g). [21]As a result of large interlayer distances of alpha form, it turns out to possess a high theoretical capacity of 433 mA/g (1558 F/g). [22]

The other important factor that affects electrochemical activity of the electrode material is the intercalating anions. In a recent study, α-$Ni(OH)_2$ was prepared following a surfactant-assisted method to control and exchange the intercalating anions. The cyclic voltammetry results demonstrated that the largest specific capacitance was obtained for the chloride-intercalated products, while the smallest value was obtained for the sulfate-intercalated case. The reasons behind this observation could be related to the anionic size differences. These results suggest that the intermolecular interactions between the intercalating anions and the layers cannot be completely ignored.

It was also demonstrated with the molecular dynamics modeling of the structures and binding energies of nickel hydroxides containing various interlayer guest anions. [23] A modified force field describing O-Ni-O angle bending and Ni-O bond stretching in nickel hydroxides is performed in this study. It introduced charges of various interlayer anions. The relative ions' binding energies calculated by Molecular Dynamic (MD) simulations can demonstrate that the relative affinity of various anions in ion exchange experiments. According to this simulation relative affinity of ions is like;

$CO_3^{2-} > SO_4^{2-} > OH^- > F^- > Cl^- > Br^- > NO_3^-$. The result of this study is related with the anion intercalated in $Ni(OH)_2$ and it can explain the interaction between $Ni(OH)_2$ and intercalated anion.

This ion affinity arrangement is also compatible with the Hofmeister series. The Hofmeister series is a classification of ions in order of their ability to salt out or salt in with the help of the hydrogen bonding. The effects of these changes were first worked out

by Franz Hofmeister, who studied the effects of cations and anions on the solubility protein. [24] The ratios for the anions follow a series from most ordered to least ordered monolayer as:

$F^- = SO_4^{2-} > HPO_4^{2-} >$ acetate $> Cl^- > NO_3^- > Br^- > ClO_3^- > I^- > ClO_4^- > SCN^-$.[25]

Early members of the series called as water structure maker (salting out) increase solvent surface tension, and decrease the solubility of nonpolar molecules. Salting out effect strengthen the hydrophobic interaction. By contrast, later salts in the series called as water structure breakers (salting in) increase the solubility of nonpolar molecules and decrease the order in water; in effect, they weaken the hydrophobic effect.

These results suggest that the intermolecular interactions between the intercalating anions and the layers cannot be ignored.

1.2.4. Methods for the Synthesis of Nickel Hydroxides

A number of chemical and electrolytic methods were attempted to synthesize $Ni(OH)_2$ powders to be employed as positive electrode materials. Portemer's group [26] electrolyzed $Ni(NO_3)_2$ solution to force precipitation of $Ni(OH)_2$ onto porous nickel electrode. Kamath and Subbanna [27] prepared reactive nickel hydroxide electrode material including direct precipitation with KOH, electrolytic precipitation, and sol-gel method. It indicates that pure $Ni(OH)_2$ can be formed by precipitation in moderately alkaline (pH<10) solutions but is unstable with respect to the α phase in contact with the battery electrolyte.

A simple mixing of nickel and hydroxide ions, using surfactants, slow release of hydroxide ions have been suggested in the literature for the synthesis of α nickel hydroxide. Although the common sense suggests a simple mixing of nickel and hydroxide ions for the facile synthesis of nickel hydroxide, the rapid supersaturation may lead to irreproducible results and a mixture of phases. [28] Therefore, alternate methods involving surfactants, slow

release of hydroxide ions, or both have been suggested in the literature. The slow release of base could be achieved by the thermal hydrolysis of urea [29,30,31] or hexamethylenetetramine (HMT) [21] . Surfactants can as well be used with hydrothermal methods for the synthesis of different forms of nickel hydroxide [21,32,33,34,35.]

Urea is an organic compound with the chemical formula $CO(NH_2)_2$. The molecule has two -NH_2 groups joined by a carbonyl (C=O) functional group. Homogeneous precipitation by urea decomposition provides opportunity to synthesize phase pure $Ni(OH)_2$ since the pH of the solution remains relatively low during the process.

Steady state level of decomposition reaction of urea is:

$$OC(NH_2)_2 \rightleftharpoons OCN^- + NH_4^+ \quad (11)$$

$$OCN^-(H^+) + 2H_2O \longrightarrow HOC_3^- + NH_4^+ \quad (12)$$

Decomposition reaction of urea is:

$$OC(NH_2)_2 + 2H_2O \longrightarrow 2NH_4^+ + CO_3^{2-} \quad (13)$$

The decomposition process in neutral media produces carbon dioxide and ammonia, which will further consume protons to form NH_4^+ and increase the hydroxide concentration [36], i. e., the pH of the solution. It has mainly been applied for the preparation of layered hydroxide salts where only one type of cation is involved.

$$M^{+2}A_y + 2\text{-}xOH^- \longrightarrow M(OH)_{2-x}(A^{m-})_{x/m} + y\text{-}xA^{m-} \quad (14)$$

In a study Akınç el al [37], homogeneous precipitation by urea decomposition provides excellent opportunity to synthesize phase pure alpha $Ni(OH)_2$ as the pH of the solution remains relatively low throughout the process. More recently, Regazzoni et al.[38] reported the synthesis by a urea method, but the average particle size is not in the nanoscale range and the shape of the particles is petal-like. In some cases of the urea method, a mixture of beta and alpha phases was obtained.

In the case of urea, hydrolysis by-products, cyanate and bicarbonate ions, also intercalate the oxide layers. The intercalated by-product may irreversibly bind to the available sites and lower the specific capacitance of the $Ni(OH)_2$.

Hexamethylenetetramine (HMT) is a heterocyclic organic compound with the formula ($C_6H_{12}N_4$). Hexamethylenetetramine is a fairly strong organic base and possesses four potential nitrogen donor atoms. Hexamethylenetetramine may react with many hydrated salts forming molecular complexes. [39] HMT may be better hydroxide source than urea since it does not have byproducts which may cause decrease in specific capacitance. Intercalated complex HMT may affect the morphology and the electrochemical properties of nickel hydroxide.

In the Jiang article, uniform hierarchical $Ni(OH)_2$ nanostructures including the flowerlike nanostructures, stacked nanoplatelets and hexagonal nanosheets have been successfully fabricated via a simple HMT-assisted hydrothermal route.[40] Among them, the flowerlike $Ni(OH)_2$ nanostructures assembled from ultrathin nanoflakesnwith diameters of 7.4 nm show the maximum specific capacitance of 1715 F/g within the potential range of 0.6 V compared with the stacked nanoplatelets (1268 F/g) and hexagonal nanosheets (1029 F/g). Although the capacitance of the nickel electrode are so high their capacity decreases immediately with the increase of cycle number.

However it is difficult to synthesize well dispersed nano-sized nickel hydroxide because of its agglomeration sonochemistry can help to synthesize well dispersed particles because of its extreme mixing conditions. Sonochemistry is taking advantage of ultrasound in chemical reactions and systems. So high intensity ultrasound can be used to facilitate the slow release of base as well as to agitate the solution during the chemical precipitation [41]

Chapter 2

2. EXPERIMENTAL

2.1. Synthesis of Nickel Hydroxide

The reactions took place in a closed glass sonication fitted system with a water jacket for temperature control. The nickel hydroxides were synthesized by the decomposition of urea and HMT under high ultrasonic medium at 80 ^{o}C and 100 ^{o}C. Thermal reactions were synthesized by thermal decomposition of urea HMT under magnetic stirrer in 80 °C controlled vessels. Both reactions were carried out under Argon gas. Analytical grade acetate, chloride, nitrate, and sulfate salts of nickel were from Sigma-Aldrich. In a typical reaction 1-16, 1-8, and 1-4 molar ratio of nickel salt to HMT were dissolved in 60 mL of deionized water. The natural pH of the solutions was around 6.0. The solution was saturated with argon for 15 min before the reaction. The solution was irradiated with the 13-mm probe of Bandelin Sonopuls HD 3200 at 20 kHz for 3 h. The ultrasonic power density was 50 W/cm^2. The temperature was kept at 80 °C and 100 °C throughout the reaction. After the precipitation process was completed, the precipitate was washed with DI water by centrifuging for 3 times. Then they were dried in 80 °C oven. Dropwise comparison samples were prepared under high ultrasonic field at 80 ^{o}C. For dropwise sample, first nickel salt was dissolved in 52 mL water and purged with argon gas. After sonication started HMT dissolved in 8 mL water added into the first sonication with the rate of 11.66 mL/hour. After the precipitation process was completed, the precipitate was washed with DI water by centrifuging for 3 times and dried in 80 °C oven.

2.2. Preparation of Electrodes

The nickel electrodes were prepared on 1×1 cm nickel foam. Nickel hydroxide (85 % by weight), acetylene black (10 % by weight), and binder Teflon (5 % by weight) were mixed with ethanol to a slurry consistency. After the transfer of slurry onto the nickel foam, the electrode was dried at 80 °C and pressed at a pressure of 1 MPa. The actual amount of nickel hydroxide on the electrode was about 4 mg.

2.3. Instrumentation

2.3.1. Ultrasonic Probe

An ultrasonic probe (Bandelin HD3200 model, 20 kHz, 200 W at 30% efficiency) with 13 mm $TiAl_6V_4$ alloy tip was used. The average intensity was on the order of 50 W/cm^2.

2.3.2. X-ray Diffraction

The powder X-ray diffraction (XRD) measurements were performed using XRD; Bruker Phaser D8. The X-ray diffraction pattern of a pure substance is, therefore, like a fingerprint of the substance. The powder XRD is an X-Ray diffraction tool enabling the analysis of poly-crystalline material. X-ray powder diffraction using the classic Bragg-Brentano geometry measures crystalline phase qualitatively and quantitatively.

An electron in an alternating electromagnetic field will oscillate with the same frequency as the field. When an X-ray beam hits an atom, the electrons around the atom start to oscillate with the same frequency as the incoming beam. The combining waves out of phase are destructive interference and there is no resultant energy leaving the solid sample. However the atoms in a crystal are arranged in a regular pattern, and in a very few directions there is constructive interference. The waves will be in phase and there will be well defined X-ray beams leaving the sample at various directions. A diffracted beam is

described as a beam composed of a large number of scattered rays that reinforce one to another.

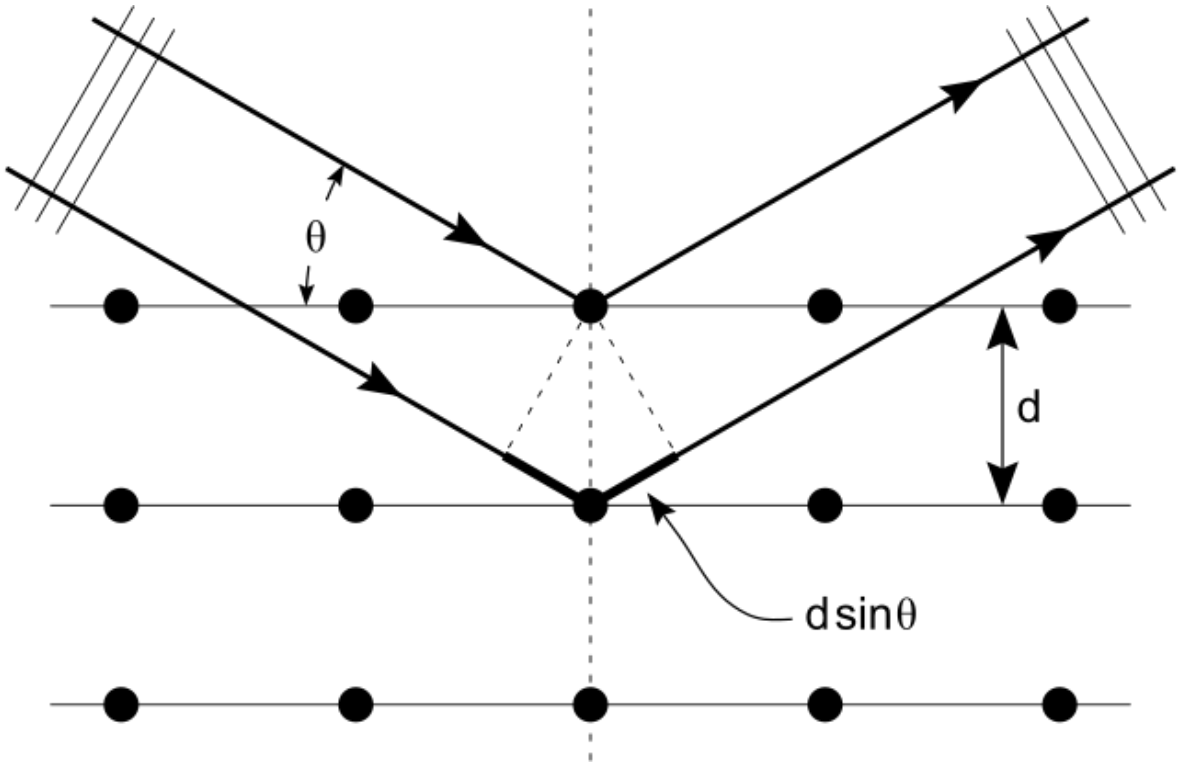

Figure 5 X-Ray Diffraction scattering

Scattered beams are arranged symmetrically with a separation d, these spherical waves can be added constructively only in directions where their path-length difference 2d sin θ equals an integer multiple of the wavelength λ. It is called Bragg Law [42] **2d sin θ = n λ** Equation 1. In that case, part of the incoming beam is deflected by an angle 2θ, producing a reflection spot in the diffraction pattern.

2d sin θ = n λ **Equation 1**

Here d is the spacing between diffracting planes, θ is the incident angle, n is any integer, and λ is the wavelength of the X-ray.

2.3.3. Infrared Spectroscopy

The samples were characterized by Fourier transform infrared (FTIR) spectroscopy (Thermo Scientific S10).

Infrared spectroscopy (IR spectroscopy) deals with the infrared region of the electromagnetic spectrum which is light with a longer wavelength and lower frequency than visible light. It is mostly based on absorption spectroscopy. It can be used to identify and study chemical groups. Molecules stretch or bend with the infrared energy and each molecular group has specific absorbance energy. The molecular group can be detected with respect to absorbed energy via IR spectroscopy. [43]

2.3.4. Scanning Electron Microscopy

Morphology of the nickel hydroxides were examined with the help of scanning electron microscope. (Zeiss Ultra Plus FE-SEM). SEM working mechanism is basically scanning the specimen with an extremely small focused electrons (a few nm in diameter). The image is produced by secondary electrons generated by the high energy electron bombardment on the sample. The intensity differences of the collected signals produce images. The brightness modulation and the depth of field adjustment help to get better picture of the specimen. The samples were not coated, and low acceleration voltages were used to avoid charging.

2.3.5. Electrochemical Characterization

The electrochemical characterization was carried out with BioLogic potentiostat. Cyclic voltammetry (CV) measurements were performed with a standard three-electrode cell system. The working electrode was prepared as follows: 85 wt.% of a $Ni(OH)_2$ sample, 10 wt.% of acetylene black and 5 wt.% of polyvinylidene difluoride were mixed in ethanol to form a homogeneous slurry. The obtained slurry was coated on clean Ni foam (1×1 cm^2) and dried at 80 °C for 12 h. The working electrodes were obtained by pressing the active material coated Ni foam at 1 MPa. The mass loading of the $Ni(OH)_2$ active material in the electrode is about 4 mg/cm^2. Nickel foam (1×1 cm^2) and the Ag/AgCl electrode were used as the counter electrode and the reference electrode, respectively. The electrolyte used for the measurement was a 6.0 M KOH solution. KOH solution is used to have basic medium electrolyte solution. The solution was purged with argon for at least 30 minutes to remove all oxygen gas in the solution. The cyclic voltammograms (CV) were recorded with a scanning rate of 50 mV/s^1. The specific capacitance values were calculated using the area under the CV curves. The area under current and time was divided to voltage range and the weight of the electrode.

Galvanostatic charge-discharge (GC) measurements were performed on BioLogic potentiostat with a three-electrode system in a 6.0 M KOH solution. The as-prepared $Ni(OH)_2$ coated Ni foam, nickel foam (1×1 cm^2) and Ag/AgCl electrode were used as the working electrode, counter electrode and reference electrode, respectively. The preparation of the working electrode is same as in the CV measurements. The GC measurements of the $Ni(OH)_2$ was performed at various charge-discharge currents 10 mA, 20 mA, 30 mA, 50 mA, 100 mA, respectively.

Their specific capacitance was calculated from charge discharge measurement according to the following equation [44] :

$$C = \frac{I}{(\Delta E / \Delta t) \times m}$$ **Equation 2**

where C_m(F/g) is the specific capacitance, I (mA) is charge–discharge current, Δt(s) is the discharging time, ΔV(V) represents the potential drop during discharge, and m(mg) is the mass of the active material within the electrode.

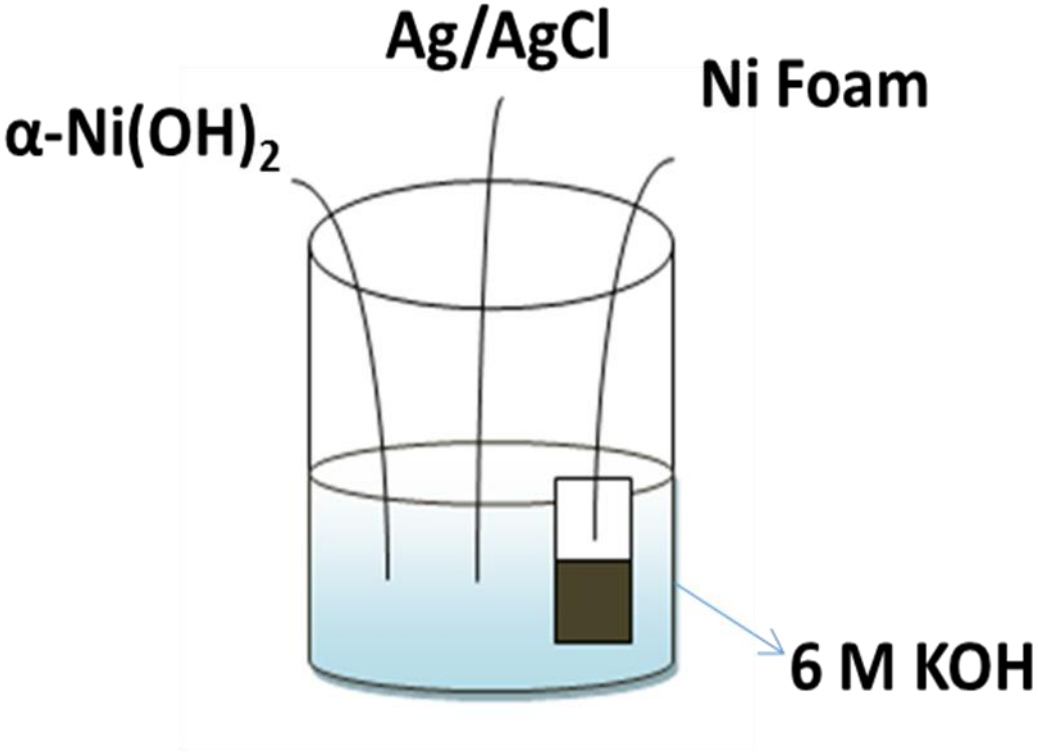

Figure 6 Three electrode system

During charging:

Oxidation Reaction /Anode Reference Reaction:

$Ni(OH)_2 \longrightarrow NiOOH + e^-$ (working electrode) (15)

Reduction Reaction / Cathode Reference Reaction

$OH^- + e^- \longrightarrow H_2O$ (16)

During discharging:

Oxidation Reaction /Anode Reference Reaction:

$H_2O \longrightarrow OH^- + e^-$ (17)

Reduction Reaction / Cathode Reference Reaction

$NiOOH \longrightarrow Ni(OH)_2 + e^-$ (working electrode) (18)

Chapter 3

3. Results & Discussion

3.1. $Ni(OH)_2$ synthesized by UREA Decomposition

3.1.1. XRD Pattern

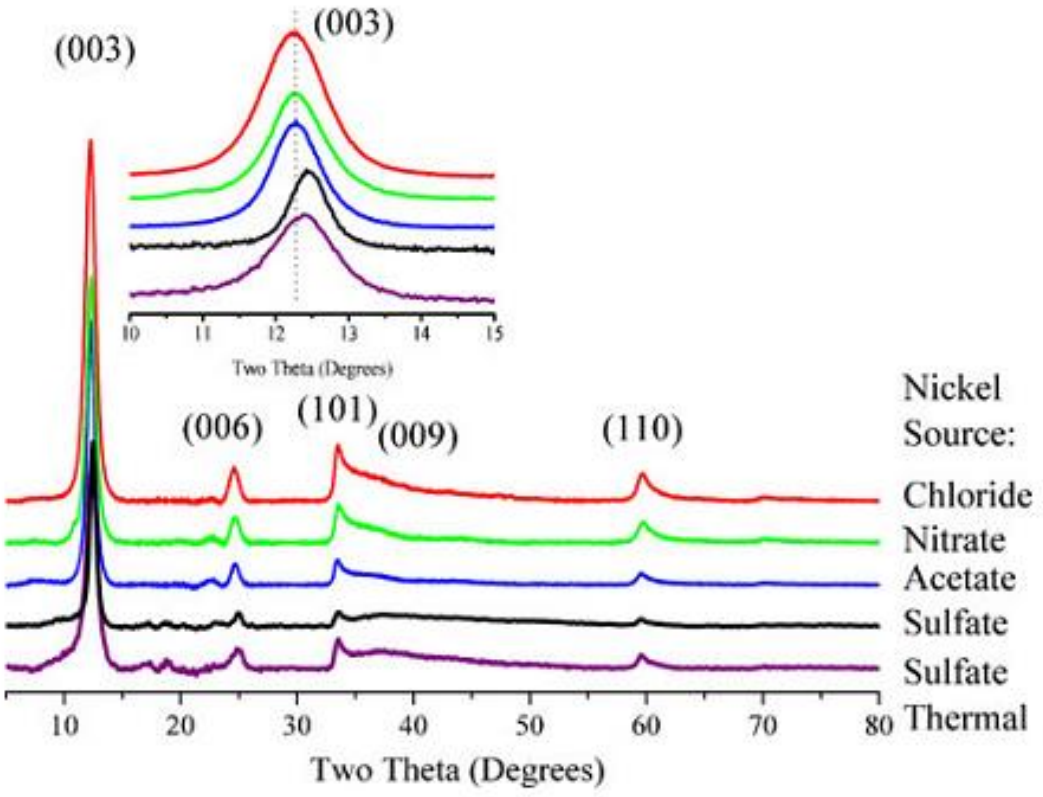

Figure 7 XRD patterns of thermally and sonochemically synthesized α-nickel hydroxides from various precursor

The XRD patterns of the α-$Ni(OH)_2$ synthesized from various nickel precursors by the sonochemical method and from nickel sulfate by the thermal method at the same temperature are presented in Figure 7.

The observed peaks at 12.44, 24.90, 33.41, and 59.51° two theta positions were identified as (003), (006), (101), and (110) peaks.

The (009) peak at 36.78° is buried under the asymmetric (101) peak in accord with the literature XRD patterns. The asymmetry of the reflection around 36° (101) indicates the formation of a turbostratic phase .

As seen in the inset, there are significant differences in the full width at half maximum (FWHM) of the (003) peak. The smallest FWHM and, consequently, the largest crystallite size were obtained for the sulfate-intercalated sample synthesized with ultrasonic irradiation in 3 hour. The FWHM of the (003) peak was calculated as 0.595° corresponding to a crystallite size of 143 Å for this sample according to .

$$\tau = \frac{K \times \lambda}{B \times \cos\theta}$$

Equation 3 Scherer's equation

On the other hand, the sample synthesized by thermal method in 18 hour has a slight shift to lower two theta values for the (003) peak, from 12.42 to 12.36°. This change was also accompanied by a decrease in the crystallite size from 143 to 83 Å. The experimental and the calculated parameters for the (003) peak are presented in Table 1.

Table 1 The (003) peak positions, FWHM values, calculated crystallite sizes, and layer spacing derived from (003) diffraction peak

Sample	Peak position(°)	FWHM (003)(°)	Crystallite size(Å)	*d*(003) spacing(Å)
Chloride US	12.25	1.05	81	7.23
Nitrate US	12.29	0.94	91	7.20
Acetate US	12.28	0.81	105	7.21
Sulfate US	12.42	0.60	143	7.13
Sulfate T-18 h	12.36	1.03	83	7.16

Among the samples prepared by the sonochemical method, the sulfate-intercalated sample stands out due to two reasons. First off, the positions of (003) and (006) peaks are shifted towards higher two theta values, and the (009) peak asymmetry is different compared to the others. The inset in Figure 7, showing the (003) peak region, demonstrates the shifts in positions clearly.

Secondly, the FWHM of the (003) peak of this sample is much narrower compared to all the other samples. As reported in Table 1, this sample has the smallest layer spacing, 7.13 Å, among the samples prepared under the same sonochemical conditions. This is a surprising result since sulfate anion has the largest radii among the used anions. For instance, in a recent study, α-cobalt hydroxide interlayer spacing was found to increase in the order of chloride, nitrate, acetate, and sulfate anions, following the size trend [46]. However, one must approach the current situation with caution due to the employment of ultrasound and the presence of cyanate ions intercalating the layers. The results presented in Table 1 can be compared with the previous studies. The alpha nickel hydroxide prepared by the thermal degradation of urea was reported to have an interlayer spacing of 7.25-7.26 Å for nitrate precursor [29,31,30,47] and 7.24 Å for chloride precursor [48]. However, utilization of

ultrasound for urea degradation has been known to shrink the interlayer spacing slightly to 7.20 Å in the case of nitrate anions [41].

3.1.2. FTIR spectra

The FTIR spectra of synthesized alpha-nickel hydroxide powders from different precursor salts are presented in **Figure 8.**

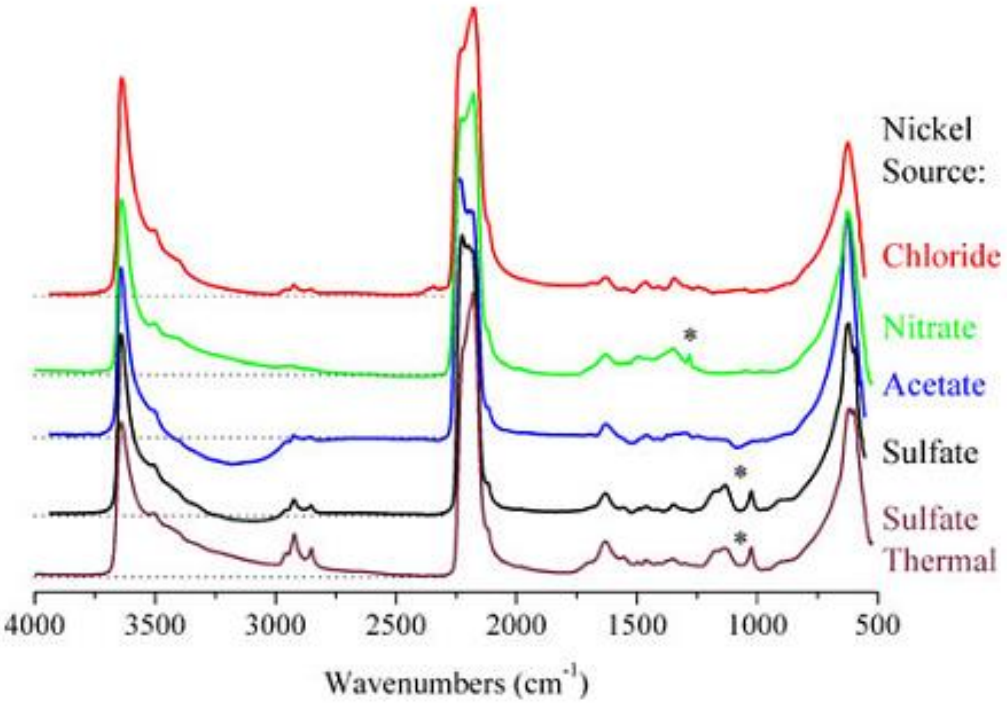

Figure 8 FTIR spectra of alpha-nickel hydroxide powders; top 4 spectra, ultrasonically from the indicated nickel salts; bottom spectrum, thermally from the sulfate salt.

The bottom spectrum belongs to the thermally synthesized product from the sulfate salt. All the other spectra are the sonochemically prepared products from the nickel salts indicated next to them. The features around 3,640 cm^{-1} are due to O–H stretching, and they are unusually sharp compared to the spectra in the literature. The sharpness of the O–H

peaks indicate “free” O–H peaks as opposed to “bound” ones as in hydrogen-bonded species [29,41,49].

The lack of significant intensity or broadening around the O–H stretching region also reduces the possibility for water molecules’ intercalation. Furthermore, the peak around 1,630 cm^{-1}, which is the bending vibrational mode of the intercalated water molecules, is quite weak compared to the spectra found in the literature. The sharp peaks around 2,200 cm^{-1} (ν_1) and 615 cm^{-1} (ν_2) belong to the cyanate (OCN^-) ion, which is a by-product of urea decomposition [48]. It should be noted that the shape of the ν_1 peak changed as the intercalating anion changed. The characteristic peaks of the sulfate and nitrate groups are indicated with an asterisk near the spectra, emphasizing that these anions did not degrade during the reaction.

A close-up of the 2,050–2,300 cm^{-1} region is presented in Figure 9, showing the deconvolution of the cyanate stretching envelopes. Since the cyanate ion was also intercalated between the layers, it could be possible to use it as a probe to gain information. A detailed assignment of the deconvoluted peaks was previously reported [48]. Accordingly, it should be possible to identify O-bonded cyanate or N-bonded iso-cyanate species and the binding sites.

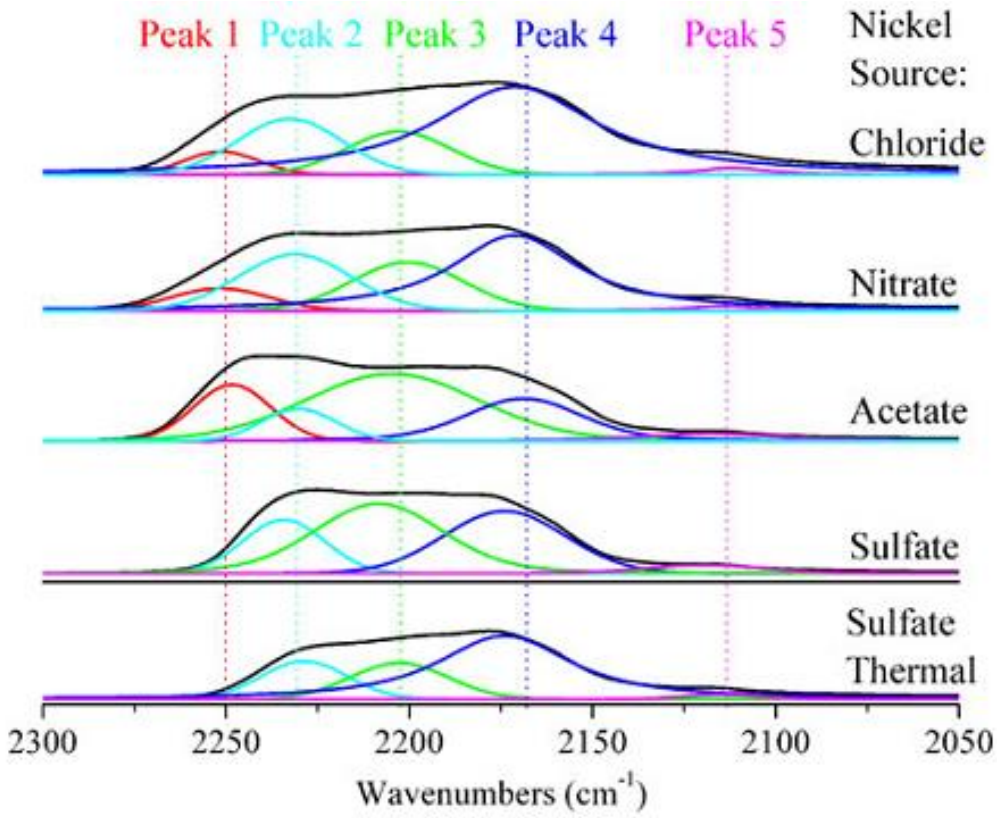

Figure 9 Deconvoluted C≡N stretching region of FTIR spectra

Following the literature assignments, the C ≡N stretching region was fitted to five peaks, and the peak parameters are presented in Table 2. The fitted peak positions agree with the previous meticulous analysis [48] except that only four peaks could be fitted in the sulfate cases. Peaks 2–4 were blue shifted about 12–14 cm^{-1} from their literature positions.

Table 2 The peak parameters and assignments for the deconvolution of the C≡N region of the FTIR spectra

	Peak 1 -OCN "atop"	Peak 2 -OCN "bridge"	Peak 3 -NCO "atop"	Peak 4 -NCO "bridge"	Peak 5 OCN "side on"
Chloride US					
Center (cm^{-1})	2,251.32	2,232.63	2,202.90	2,171.20	2,111.75
Area (%)	5.1	17.2	13.2	62.4	2.1
FWHM (cm^{-1})	24.1	33.7	33.6	53.3	22.6
Nitrate US					
Center (cm^{-1})	2,251.59	2,231.29	2,200.51	2,171.28	2,114.35
Area (%)	7.6	22.3	19.1	49.3	1.7
FWHM (cm^{-1})	31.3	36.1	36	41.3	22.6
Acetate US					
Center (cm^{-1})	2,248.35	2,230.11	2,204.72	2,168.83	2,118.11
Area (%)	16.5	9.1	46.6	21.7	6.0
FWHM (cm^{-1})	24.7	24.0	49.5	37.5	44.8
Sulfate US					
Center (cm^{-1})	–	2,234.26	2,208.46	2,174.02	2,119.53
Area (%)	–	19.0	43.1	33.3	4.6
FWHM (cm^{-1})	–	26.2	41.6	39.0	39.0
Sulfate T					
Center (cm^{-1})	–	2,228.62	2,202.75	2,174.01	2,114.87
Area (%)	–	17.1	18.6	62.3	2.0
FWHM (cm^{-1})	–	27.7	31.7	43.0	26.2

Peak 1 around 2,250 cm^{-1} was identified as O-bonded cyanate at "atop" position, i.e., unidentate on top of a nickel atom. This peak was missing for the sulfate cases. Peak 2 around 2,230 cm^{-1} was assigned to O-bonded cyanate at "fourfold" bridge position. Peak 3 located ca. 2,200 cm^{-1} was identified as N-bonded isocyanate at atop position. Peak 4, observed around 2,170 cm^{-1}, was assigned as N-bonded isocyanate at "bridge," i.e., bidentate between two nickel atoms or fourfold position. Peak 5 around 2,115 cm^{-1} was assigned for the "side-on" attachment of the anion. The deconvolution of the chloride-intercalated product's spectrum can be compared to a previous report [30], keeping in mind

that although the anion was the same, previous study did not utilize ultrasound. The C≡N stretching region in the present work was dominated by peak 4, i.e., bridge isocyanate, whereas the major contributor was peak 1, i.e., atop cyanate, in the reported work [30]. There are also subtle differences between the thermally and ultrasonically prepared sulfate-intercalated samples. In addition to the lack of "peak 1" in the deconvolution of the cyanate peaks, there is also a clear shift for the isocyanate ion from the bridge position to atop position for the thermally prepared sample. This change contradicts the general trend in the present study; with increasing size of the intercalated anions, from chloride to nitrate to acetate, the contributions shifted from the bridge to atop positions, as indicated by the intensity shifting from peak 4 to 3 and from peak 2 to 1.Further inspection reveals that the broad structure in the O–H stretching region is slightly narrower for the ultrasonically prepared sample. Dotted baselines were placed in the figure to guide the eye. This narrowing behavior is also paralleled by the weaker intensity of the 1,630 cm^{-1} peak, i.e., the bending mode of the intercalated water.

3.1.3. Morphology

The anion of the precursor salts altered the morphology of the products significantly as observed in the scanning electron microscopy (SEM) images presented in Figure 10. The alpha-nickel hydroxide thermally synthesized from the sulfate salt had an extended flower-like structure. Utilization of ultrasound altered the morphology to 2–3 mm large spherical structures for this precursor. A careful inspection revealed that the thicknesses of layers forming the structures increased with ultrasound. The product synthesized by the sonochemical degradation of urea from the acetate precursor had 5–6 mm large spherical particles composed of "cornflake"-like pieces. The chloride anion caused these cornflake-like sheets to generate extended structures instead of spherical clusters. The nitrate anion,

on the other hand, formed submicron-sized spheroids like the sulfate case; however, the flake thicknesses were much smaller compared to the sulfate case.

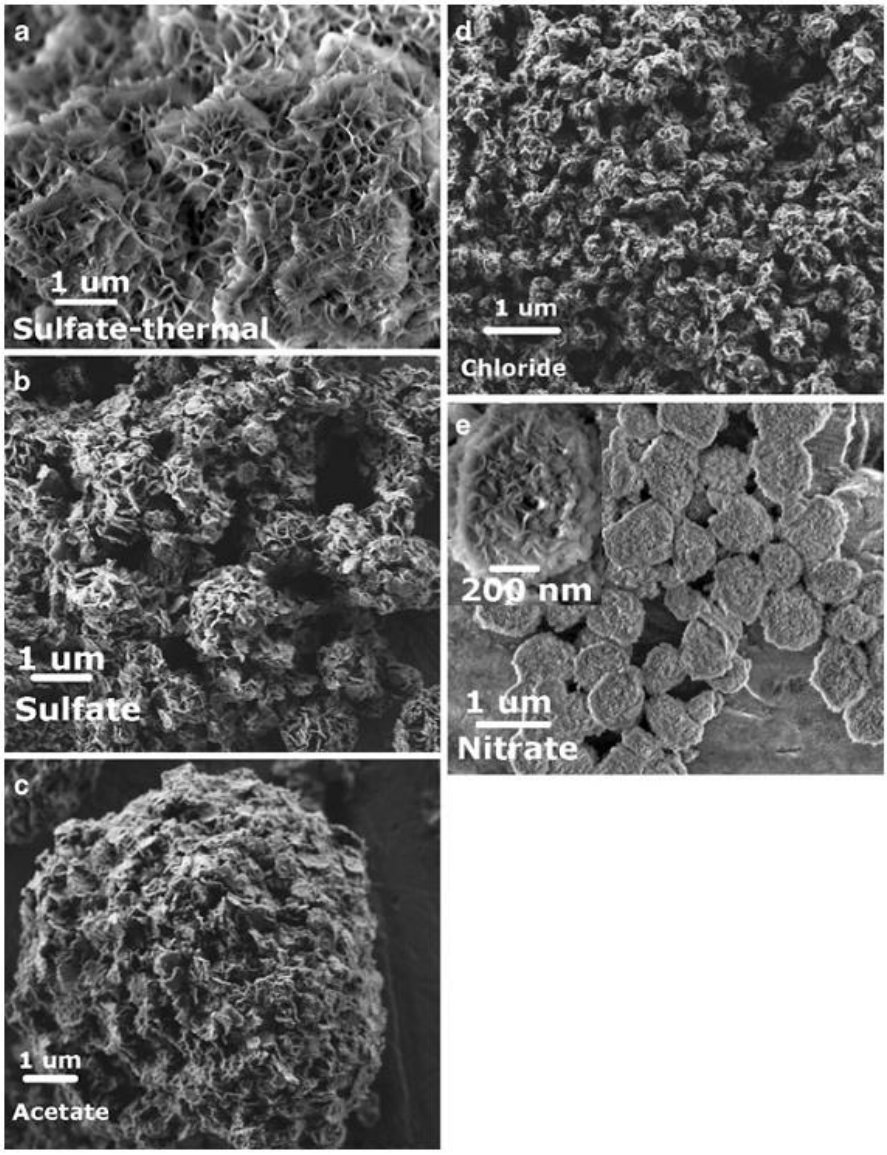

Figure 10 SEM images of alpha-nickel hydroxides

3.1.4. Electrochemical analysis

The cyclic voltammograms of the samples recorded in 6 M KOH solutions at a sweep rate of 50 mV/s are presented in Figure 11. As seen in the figure, only two peaks were observed for all samples. Anodic peak (positive current density) is assigned to oxidation of Ni^{2+} to Ni^{3+}, and the cathodic peak is the reverse reaction.

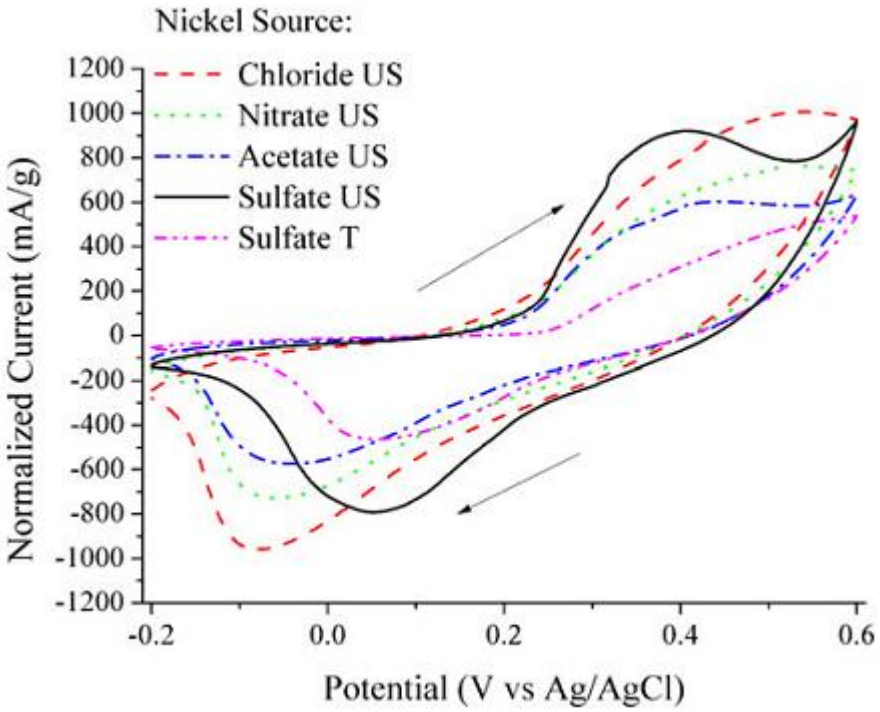

Figure 11 Cyclic voltammograms (tenth cycle) of alpha-nickel hydroxides synthesized from different salts.

The shapes of the CVs are distinguishable from the ideal rectangular shape observed for electrical double-layer capacitance. The peaks observed in the CVs can be identified as the result of a fast and reversible redox process accompanied by an

intercalation/deintercalation reaction that occurs at the interface of the film and electrolyte according to the reaction given in Lee et al. [21].

$$Ni(OH)_2 + OH^- \longleftrightarrow NiOOH + H_2O + e^- \quad (19)$$

Oxidation process occurs via deintercalation of water, proton/hydronium, and anions from the interlayer, while hydroxyl ions are intercalated during the process. In addition, chemical aging of the film in an alkali solution as well as electrochemical aging between oxidized and reduced species are also present with the redox reaction. It is quite obvious from the CV curves that interlayer anion influences the electrochemical behavior. The largest area could be obtained for the Cl-intercalated samples. The area under the nitrate-intercalated sample is slightly larger than the acetate-intercalated sample. There is, however, quite a difference between the thermally and ultrasonically prepared sulfate-intercalated samples. The ultrasonically prepared sample has not only a more noticeable oxidation peak but also a curve that is almost twice the area compared to the thermally prepared sample. Furthermore, the area under this sample is larger compared to that of nitrate- and acetate-intercalated samples. This observation contradicts the previous reports for alpha-nickel[21] and alpha-cobalt hydroxide[46] samples prepared by homogenous precipitation; the area under the CV curve of the chloride-intercalated sample was reported to be the largest, and that of sulfate was the smallest. The specific capacitance can be calculated from the area under the CV curve according to the following equation[21]:

$$C = \frac{1}{mv\Delta V}\int_{V_i}^{V_f} I(V)dV \quad \textbf{Equation 4}$$

Where m is the mass of the active material, v is the scan rate, ΔV is the potential window in which the potential was scanned between potential limits of the voltammetric curve, V_f and v_i. The specific capacitance values calculated for the 50 mV/s scan rate are 258, 195, 159, and 223 F/g for chloride-, nitrate-, acetate-, and sulfate-intercalated ultrasonic samples, respectively. The calculated specific capacitance for thermally prepared sulfate-intercalated sample was only 118 F/g. However, the 90 % increase in the specific capacitance of the sulfate-intercalated sample due to ultrasound-assisted preparation is highly significant.

One of the distinct features of the CV curves in Figure 11 is the difference between positions of the anodic and cathodic peaks for $Ni(OH)_2$ intercalated with different anions. The difference between the anodic and cathodic peaks can give information about the reversibility of the redox reaction, and the smaller is the difference between these two peaks, the more is the reversibility of the redox reaction. The redox peak positions and differences are provided in Table 3.

As seen in the figure, utilization of ultrasound not only significantly increased the area under the curve but has shifted the redox potentials for the sulfate-intercalated sample, as well. As a result, α-nickel hydroxide synthesized ultrasonically from sulfate precursors has reached the highest reversibility. These samples also showed the highest performance in terms of charge efficiency, which is judged by the difference between the oxidation peak of the Ni^{2+} and oxidation potential of water. Well-separated oxidation peak of Ni^{2+} from the oxygen evaluation peak means that the Ni^{2+} is oxidized before oxygen starts to evaluate from water.

Table 3 The specific capacitance values and redox potentials of samples

	Specific Capacitance (F/g)	Oxidation Potential(V)	Reduction Potential(V)	ΔV_o *(V)	ΔE**(V)
Chloride US	258	0.54	-0.08	0.62	0.06
Nitrate US	195	0.53	-0.07	0.60	0.07
Acetate US	159	0.44	-0.04	0.48	0.16
Sulfate US	223	0.42	0.05	0.37	0.18
Sulfate T	118	0.56	0.05	0.51	0.04

*$\Delta V_o = V_{oxidation} - V_{reduction}$ REVERSIBILITY

** $\Delta E = V_{oxidation\ of\ water} - V_{oxidation}$ CHARGE EFFICIENCY

3.2. $Ni(OH)_2$ synthesized by HMT Decomposition

3.2.1. XRD Pattern

XRD pattern of nickel hydroxide powders ultrasonically synthesized from the sulfate precursor at different nickel salts to HMT ratios at 80 ^oC was represented in Figure 12. All ratios (1:4, 1:8, and 1:16 nickel salts to HMT) yield pure alpha form of the nickel hydroxide.

The observed peaks for sulfate precursors around at 11, 23, 34, and 60° two theta positions were identified as (003), (006), (101), and (110) peaks, respectively for alpha form of nickel hydroxide. The best crystalline structure was obtained with the ratio 1-8. For 1-4 ratios, the peaks are broad. Broad peaks did not mean amorphous materials since amorphous materials do not possess periodicity. That means there would me more than one peak under the broad peaks indicating the nanoscale dimensionality of the crystallites. In general, the broadening of XRD peaks may result from small grain sizes or structural micro distortions in the crystal. Under our experimental conditions, the extremely small particle structure results in a significant broadening of the diffraction peaks in the XRD pattern of $Ni(OH)_2$. [50] For 1-16 ratios, the intensities of the peaks identifying alpha form are (003), (006) low. Although sulfate-US-(1-16) had the highest crystallite size, sulfate-US-(1-8) was used for other precursors (acetate, nitrate, and chloride) as the ratio of nickel to HMT.

Table 4 The (003) peak positions, FWHM values, calculated crystallite sizes, and layer spacing derived from (003) diffraction peak for Sulfate-US-(1-4),Sulfate-US-(1-8), Sulfate-US-(1-16)

	peak position (^{o})	**FWHM (^{o})**	**crystallite size (Å)**
Sulfate-US (1-4)	10.85	2.534	32.9
Sulfate-US (1-8)	10.54	2.449	34.1
Sulfate-US (1-16)	10.70	2.283	36.5

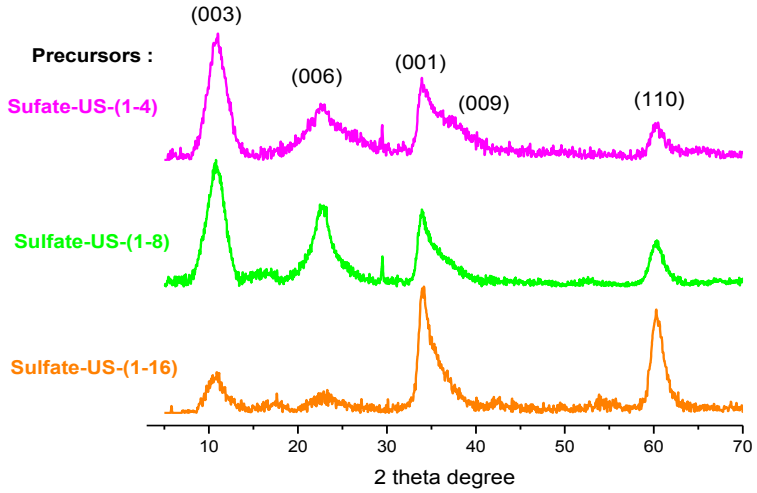

Figure 12 XRD pattern of nickel hydroxide powders ultrasonically from the sulfate precursor at different nickel salts to HMT ratios at 80 ^{o}C.

The XRD patterns of the $Ni(OH)_2$ synthesized from various nickel precursors by the sonochemical method, dropwise sonochemical method, and the thermal method at the same temperature (80 ^{o}C) and nickel-HMT (1-8) ratio are presented in Figure 13. All sulfate precursor methods yields pure alpha form of the nickel hydroxide. On the other hand for the other precursors, there were 2 different layered structure of alpha form. For the acetate, chloride and nitrate precursors, the first reflection for nickel hydroxide appears around at 7^{o} (2θ) and its harmonic at around 14^{o} (2θ). These two harmonic peaks prove that there is layered structure.[36] The other peaks come from the originated alpha form of nickel hydroxide. So there were two phase of layered alpha nickel hydroxide.

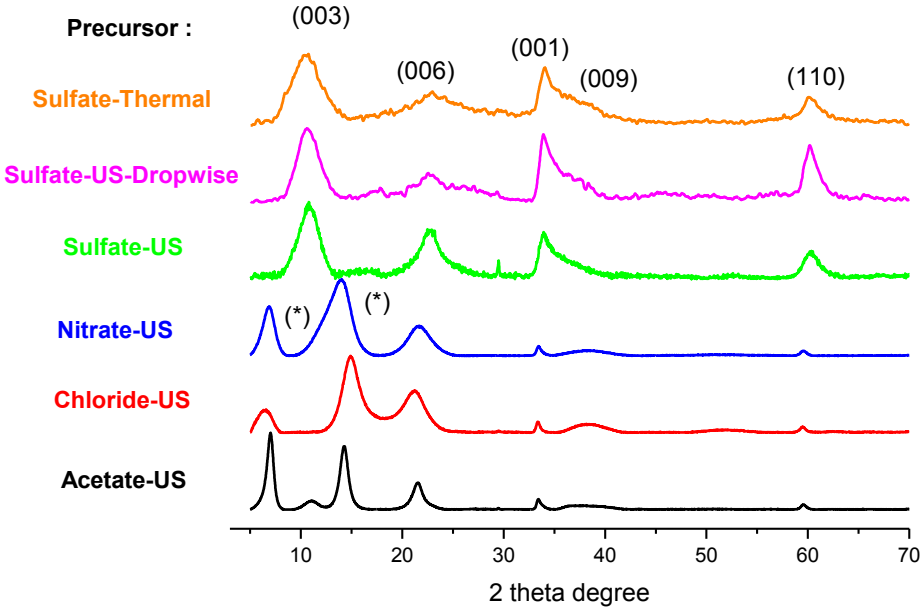

Figure 13 XRD patterns of thermally and sonochemically synthesized nickel hydroxides from various precursors at 80 ºC.

Table 5 The (001) peak positions, FWHM values, calculated crystallite sizes, and layer spacing derived from (001) diffraction peak for Acetate-US, Chloride-US, and Nitrate-US; The (003) peak positions FWHM values, calculated crystallite sizes, and layer spacing derived from (003) diffraction peak for Sulfate-US, Sulfate-US-Dropwise, and Sulfate-Thermal.

	peak position (º)	**FWHM (º)**	**crystallite size (Å)**	**d spacing (Å)**
Acetate-US	14.27	0.932	85.9	6.19
Chloride-US	14.93	1.842	43.5	5.92
Nitrate-US	13.67	2.801	28.6	6.46
Sulfate-US	10.82	2.132	34.5	8.16
Sulfate-US-Dropwise	10.72	2.52	31.7	8.24
Sulfate-Thermal	10.64	3.219	24.8	8.30

There were small differences as seen in Table 5. This observation could be related to the anionic size differences in aqueous medium. These results can be attributed to the degree of disturbance in the structure which is influenced by the anion diameter which has order as;

SO_4^{2-}(516 pm)> Cl^-(368 pm) > NO_3^-(358 pm) >CH_3COO^{--}(324 pm).[51]

It can be also explained that chloride has about 0.318 nm Cl-O distance, nitrate has about 0.345 nm N-O distance, acetate has about 0.35-0.37 nm C-O distance, acetate anion poses special difficulties, due to its nonsymmetrical nature, having a hydrophilic end and a hydrophobic end, and finally sulfate has 0.38 nm S-O distance. [52] Chloride intercalated sample has the lowest d-spacing while sulfate has the highest d-spacing which is in same order with the anion size of acetate, chloride, sulfate and nitrate. These results could be related with anion diameter.

On the other hand the net charge of the anion and the van der Waals radius of intercalated anion both affect the spacing of the interlayer nickel hydroxides. Only sulfate precursor has charge of 2-. It has one phase pure alpha form and highest d-spacing.

The interlayer water molecules in $Ni(OH)_2$ containing NO^{3-}, Cl^-, and ,CH_3COO^- are closely packed.[25] So the interlayer spacing distance is less for these ions compared to the SO_4^{2-} ion.

It has been demonstrated that various anions such as CO_3^{2-}, SO_4^{2-}, OH^-, F^-, Cl^-, Br^-, and NO_3^- are able to enter the interlayers of the-$Ni(OH)_2$ and the relative affinity of the layers toward these anions follows the order: CO_3^{2-}>SO_4^{2-}>OH^->F^->Cl^->Br^->NO_3^-.[53] According to Molecular Dynamic (MD) simulation relative affinity of ions is like; SO_4^{2-} >Cl^- > NO_3^-. [23] In MD simulations, α-$Ni(OH)_2$, β-$Ni(OH)_2$, and Ni/Al-layered double hydroxides (LDHs) have been performed in order to study structures and binding energies of the materials containing various anions such as CO_3^{2-}, SO_4^{2-}, OH^-,F^-,Cl^-,Br^-, and NO_3^-. They proposed a modified force field of the cff91 form with the introduction of a double-well potential for

describing oxygen-metal-oxygen angle bending. It demonstrated that sulfate anion has the highest relative affinity in ion exchange in Ni-O field. This simulation also explains why sulfate has the highest d-spacing.

Ultrasonicated sulfate precursor has the highest crystallite size as 34.5 Å, ultrasonically dropwise just has 31.7 Å, and thermal has the lowest one as 24.8 Å crystallite size according to (003) peak for sulfate precursor.

HMT decomposes well at higher temperature and nickel hydroxide synthesized by decomposition of HMT is done higher temperature than 80 ^{o}C.[35, 49, 54] For the next experiments, the temperature of the experiment increased to 100 ^{o}C instead of 80 ^{o}C.

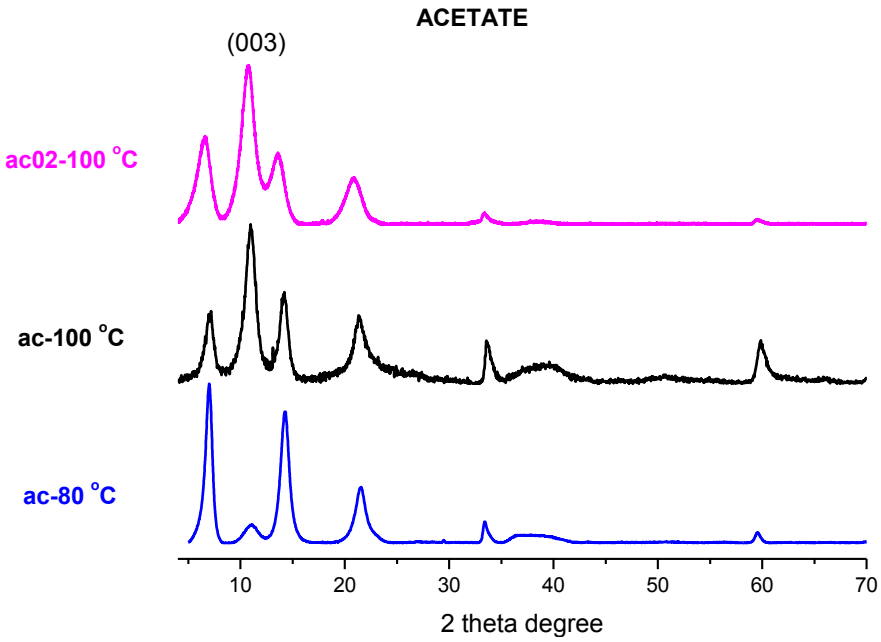

Figure 14 XRD patterns of sonochemically synthesized alpha-nickel hydroxides from acetate precursor at different temperature.

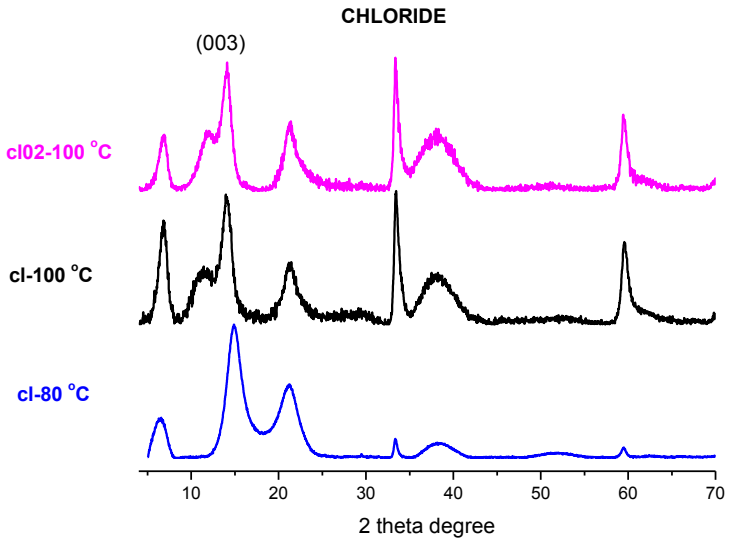

Figure 15 XRD patterns of sonochemically synthesized alpha-nickel hydroxides from chloride precursor at different temperature.

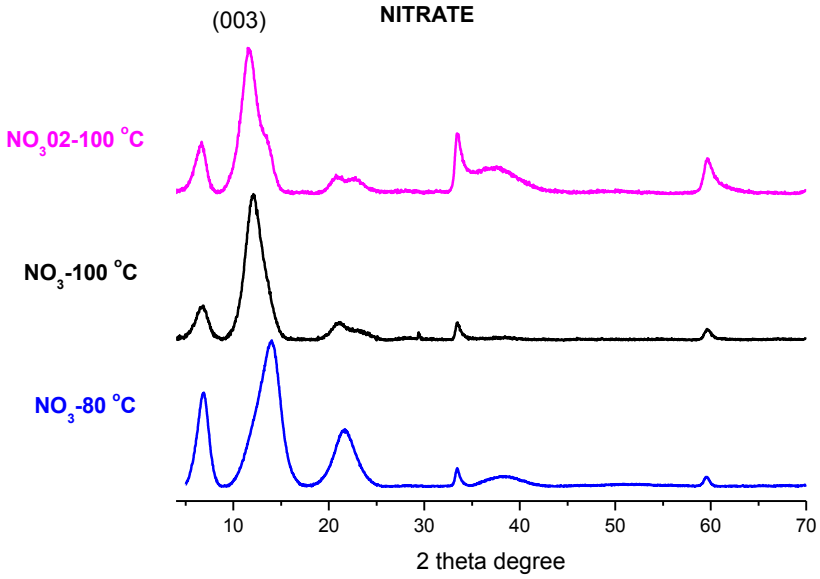

Figure 16 XRD patterns of sonochemically synthesized alpha-nickel hydroxides from nitrate precursor at different temperature

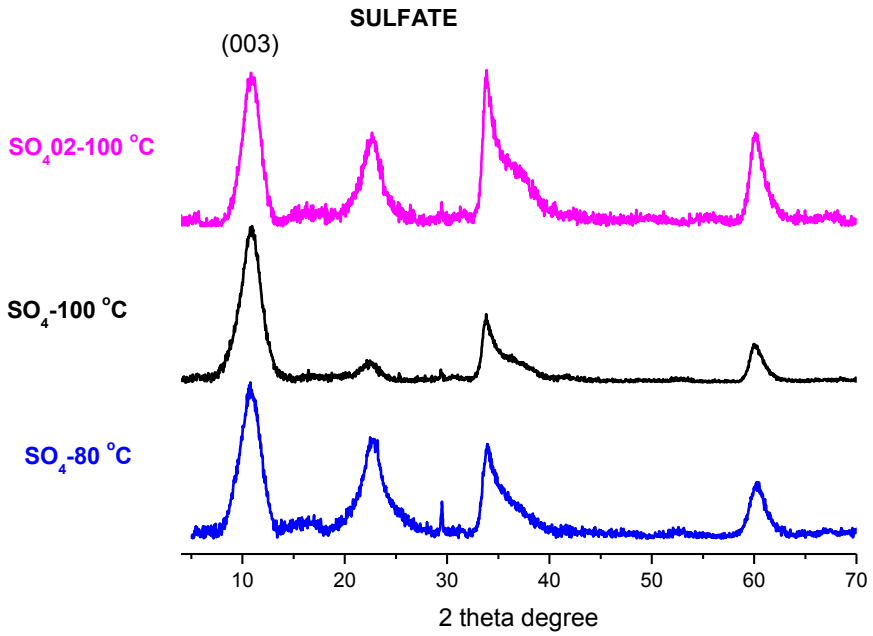

Figure 17 XRD patterns of sonochemically synthesized alpha-nickel hydroxides from sulfate precursor at different temperature.

Table 6 The (003) peak positions FWHM values, calculated crystallite sizes, and layer spacing derived from (003) diffraction peak for all precursors.

	peak position (º)	**FWHM (º)**	**crystallite size (Å)**	**d-spacing (Å)**
Acetate-US-100 ºC	10.98	1.32	61.25	8.05
Chloride-US-100 ºC	11.62	0.77	103.00	7.61
Nitrate-US-100 ºC	11.66	2.01	39.76	7.58
Sulfate-US-100 ºC	10.71	1.94	43.21	8.25

XRD patterns of these samples also present typical peaks for α-$Ni(OH)_2$, the d value of the 003 peak ranges from 7.58 to 8.25 Å. The peaks look almost same with 80 ºC reactions for sulfate precursors. For other precursors and the position of the 003 peaks were also shifted. This phenomenon may be induced by the extent of intercalating organic molecules which were byproduct of HMT in the layered structure of the α-$Ni(OH)_2$. No peaks for β-$Ni(OH)_2$ can be observed in these XRD patterns shown in Figure 14, Figure 15, Figure 16, Figure 17. The asymmetric nature of the reflection at about 35º 2θ indicates the formation of a turbostratic phase observed in most of the α-type hydroxides, corresponding to the formation of α-form of nickel hydroxide.[49] if some metal cations in the brucite-like sheets adopt the trivalent state, anions from the solution will then be intercalated into the intersheet space (interlayer space) to maintain charge neutrality for the solid, [55] which leads to the formation of hydrotalcite-like structure (named after the natural hydrotalcite compound (Mixed metal hydroxides with hydrotalcite structure, $[M^{2+}_{1-x}M_x^{3+}(OH)_2]A^{n-}_{x/n}\cdot mH_2O)$. [56] The entire small peaks around (003) peaks may display hydrotalcite-like features.

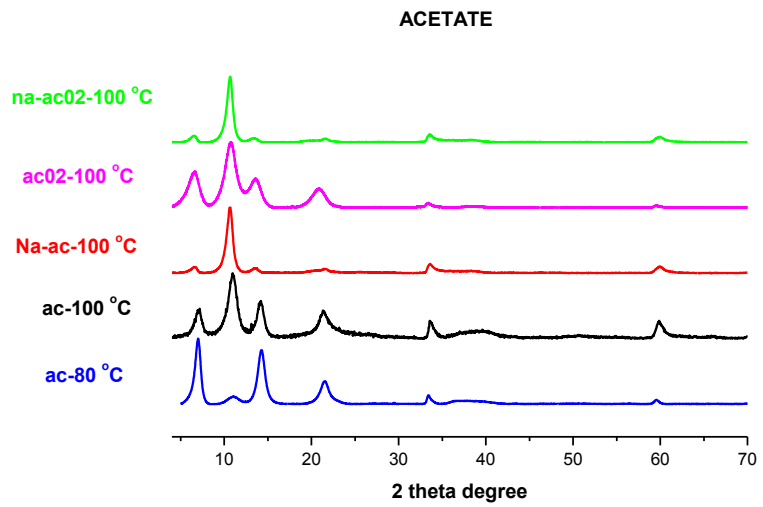

Figure 18 XRD patterns of sonochemically synthesized alpha-nickel hydroxides from acetate precursor at different temperature and addition of extra acetate ion

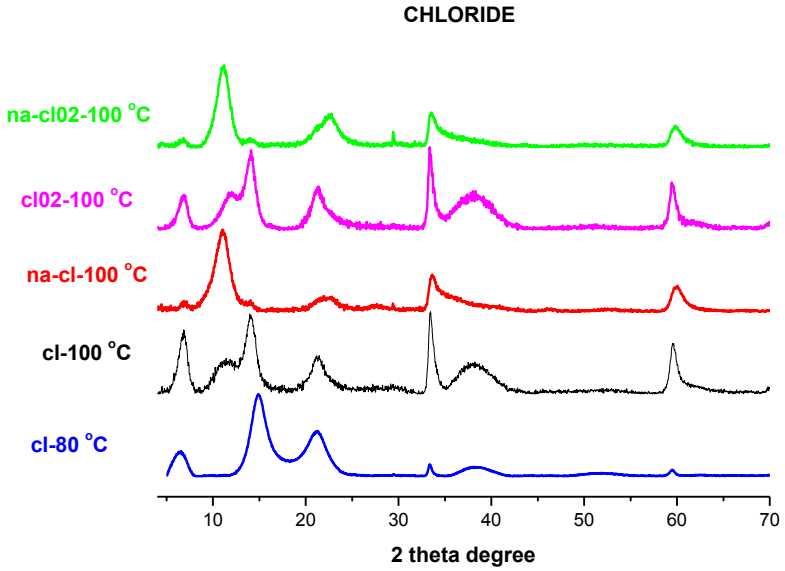

Figure 19 XRD patterns of sonochemically synthesized alpha-nickel hydroxides from chloride precursor at different temperature and addition of extra acetate ion.

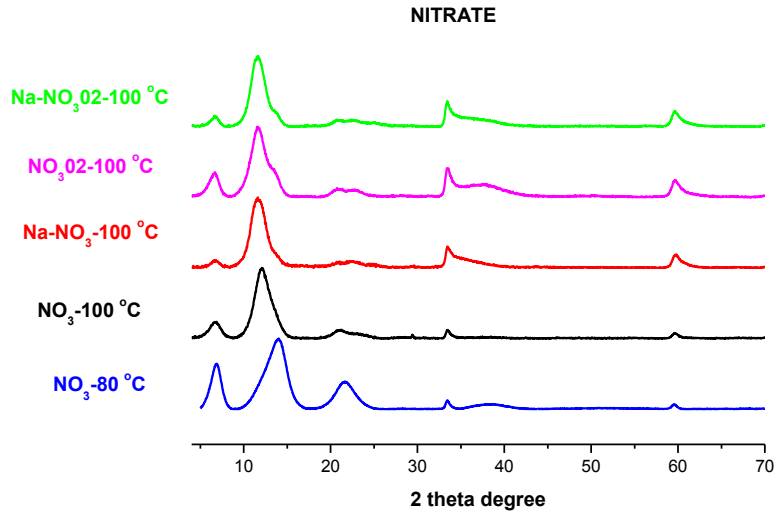

Figure 20 XRD patterns of sonochemically synthesized alpha-nickel hydroxides from nitrate precursor at different temperature and addition of extra acetate ion.

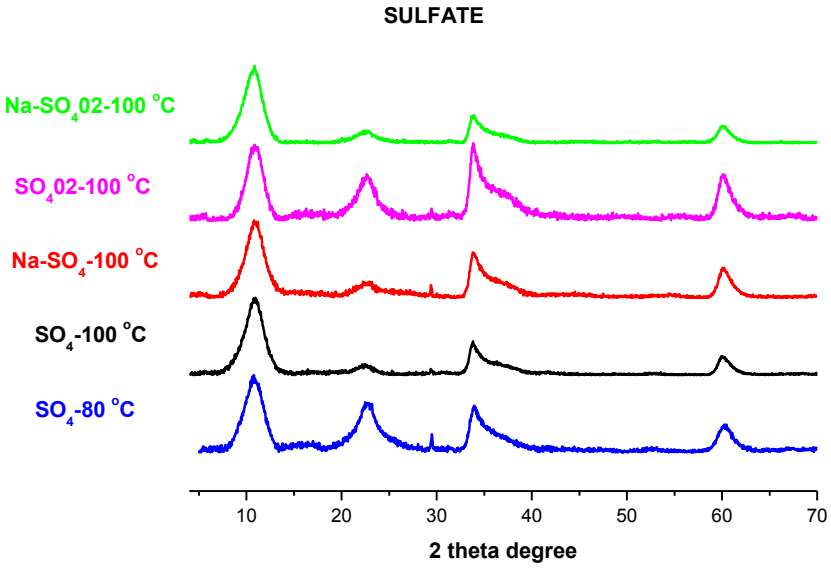

Figure 21 XRD patterns of sonochemically synthesized alpha-nickel hydroxides from nitrate precursor at different temperature and addition of extra acetate ion.

Table 7 The (003) peak positions FWHM values, calculated crystallite sizes, and layer spacing derived from (003) diffraction peak for all precursors.

	peak position (º)	**FWHM (º)**	**crystallite size (Å)**	**d-spacing (Å)**
Acetate-US-100 ºC	10.98	1.32	61.25	8.05
Na-Acetate-US-100 ºC	10.76	0.79	82.34	8.21
Chloride-US-100 ºC	11.62	0.77	103.00	7.61
Na-Chloride-US-100 ºC	11.11	1.51	52.98	7.95
Nitrate-US-100 ºC	11.66	2.01	39.76	7.58
Na-Nitrate-US-100 ºC	11.55	1.88	43.50	7.65
Sulfate-US-100 ºC	10.71	1.94	43.21	8.25
Na-Sulfate-US-100 ºC	10.68	2.21	46.78	8.27

For each precursor acetate, chloride, nitrate and sulfate sonicated at 100 ºC extra anion was added to test whether adding extra anion would affect intercalation or not in Figure 18, Figure 19, Figure 20, Figure 21. If adding extra anion lead intercalation more the electrochemical properties of nickel hydroxide would improve. Extra anion addition caused shift to the lower 2θ degree. d-spacing of the nickel hydroxide was also increased with the addition of extra anion. The spacing of the nickel hydroxide increased since more anion intercaleted with the increase of the anion concentration.

3.2.2. FTIR spectra

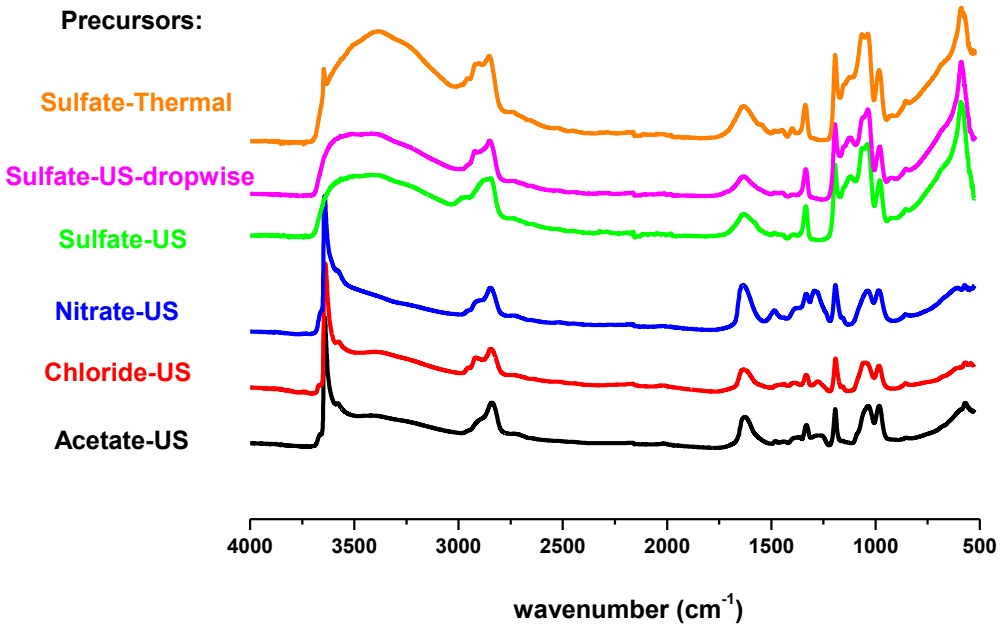

Figure 22 FTIR spectra of nickel hydroxide powders; bottom 5 spectra, ultrasonically from the indicated nickel salts; top two spectra, dropwise sonicated and thermally from the sulfate salt at 80 ^{o}C.

FTIR studies have been carried out to characterize $Ni(OH)_2$. The FTIR spectra of the $Ni(OH)_2$ synthesized from various nickel precursors by the sonochemical method, dropwise method and the thermal method at the same temperature are presented in Figure 22. The top spectrum belongs to the thermally synthesized product from the sulfate salt. All the other spectra are the sonochemically prepared products from the nickel salts indicated next to them.

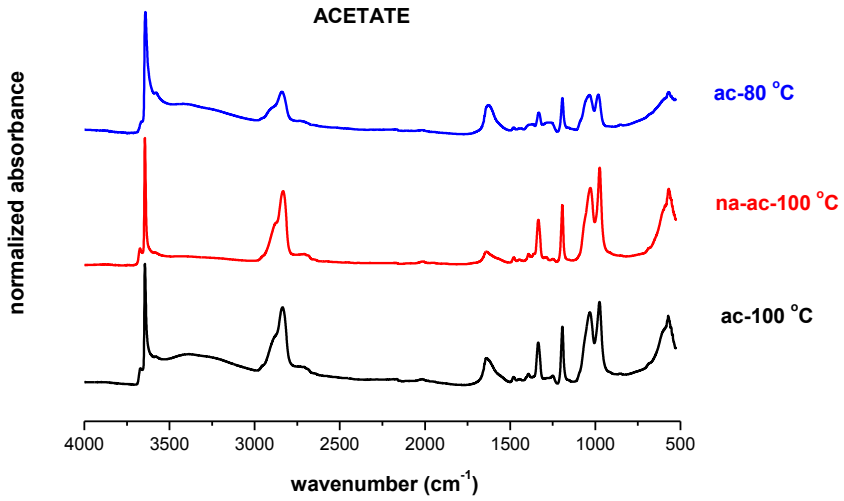

Figure 23 FTIR spectra of nickel hydroxide powders from acetate precursor.

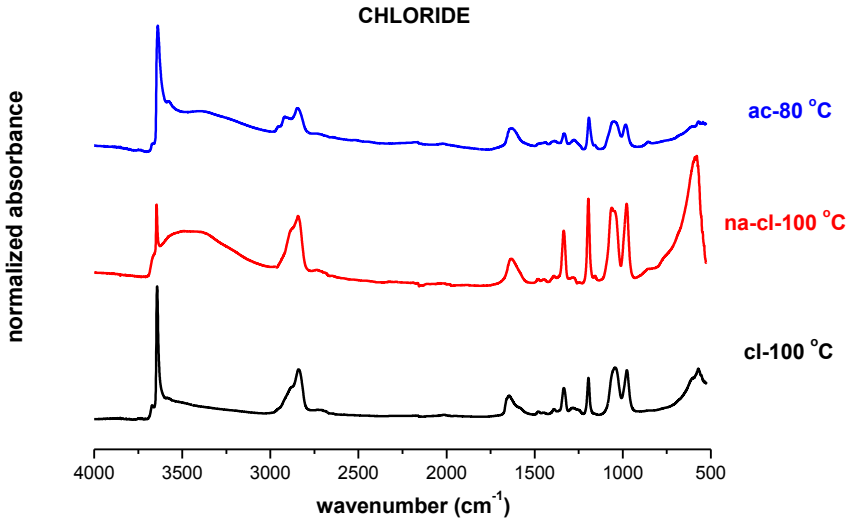

Figure 24 FTIR spectra of nickel hydroxide powders from chloride precursor.

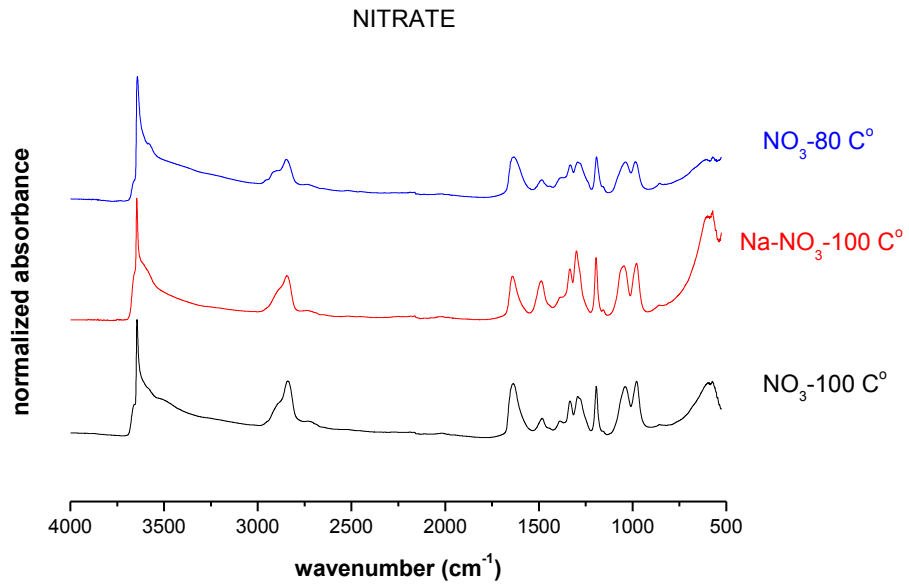

Figure 25 FTIR spectra of nickel hydroxide powders from nitrate precursor.

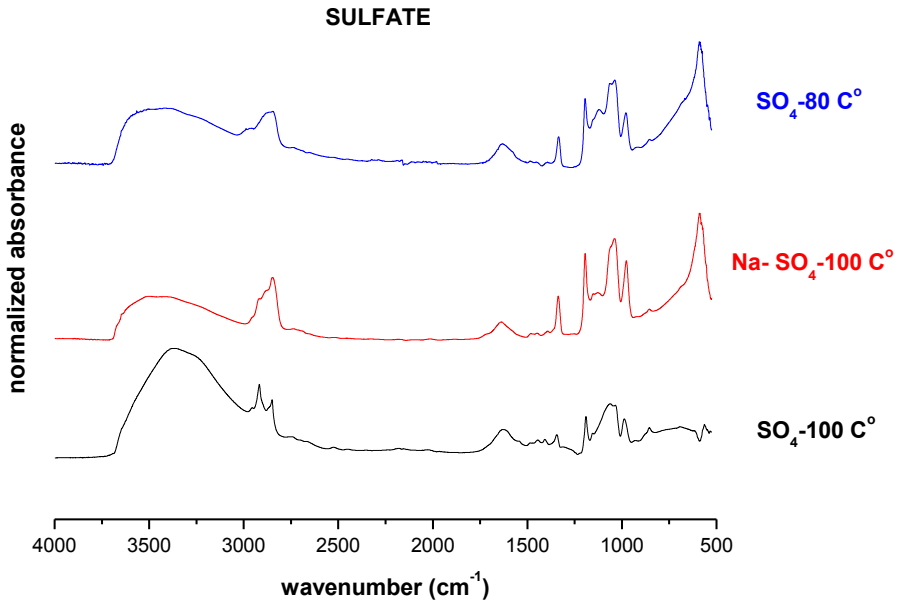

Figure 26 FTIR spectra of nickel hydroxide powders from nitrate precursor.

The sharp band at 3633 cm^{-1} is due to free O–H stretching in Figure 23, Figure 24, Figure 25. α- Ni $(OH)_2$ has also broad intercalated O-H stretching at 3250-3600 cm^{-1} range clearly seen in Figure 26. Medium intensity peaks at 2830 cm^{-1} and 2900 cm^{-1} correspond to C-H stretching. The peak at 1630 cm^{-1} refers free O-H bending coming from intercalated water and 1290 cm^{-1} wavelength refers C-H bending. Except free O-H stretching at 3633 cm^{-1}, all peak mentioned above show up in all precursors both pure alpha and 2 phase alpha phases of nickel hydroxide. [20]

For the sulfate precursors synthesized ultrasonically, thermal, and dropwise ultrasonically, all have very weak peak at 685 cm^{-1} (ν_2 mode, medium intensity peak ah 860 cm^{-1} (ν_4+ lattice mode combination), and 1065 cm^{-1} (ν_1 mode) which are coming from SO_4^{-2} band. This indicates that sulfate ion is in interlayer space. For the nitrate precursor, medium intensity peaks at 1280 cm^{-1} (ν_3 mode), 1310 cm^{-1} (ν_3 mode), and 1340 cm^{-1} (ν_3 mode) wavelengths indicate the nitrate presence in the interlayer space. [20]

Only the difference for the FTIR spectrum was because of the intercaled anion. Temperature increase and the addition of the extra anion in to the reaction did not affect the FTIR spectra.

3.2.3. Morphology

The scanning electron microscopy images in Figure 27 shows that only the sulfate precursors both sonicated and dropwise sonicated at 80 ºC are composed of extended flower like spherical shape. Other precursors; acetate, chloride, and sulfate thermal at 80 ºC have bulk sheet structure. It was also morphologically proved that sulfate precursor yields pure alpha form and others yield mixture of 2 phase of alpha form of nickel hydroxide. For the thermal degradation of HMT, the porous sheets are observed but they are not spherical particles.

In the previous study, synthesis of $Ni(OH)_2$ by urea, [7] all nickel hydroxide particles synthesized from different precursors were "cornflake"-like pieces . $Ni(OH)_2$ synthesized by degradation of HMT yield totally different morphology the degradation of urea.

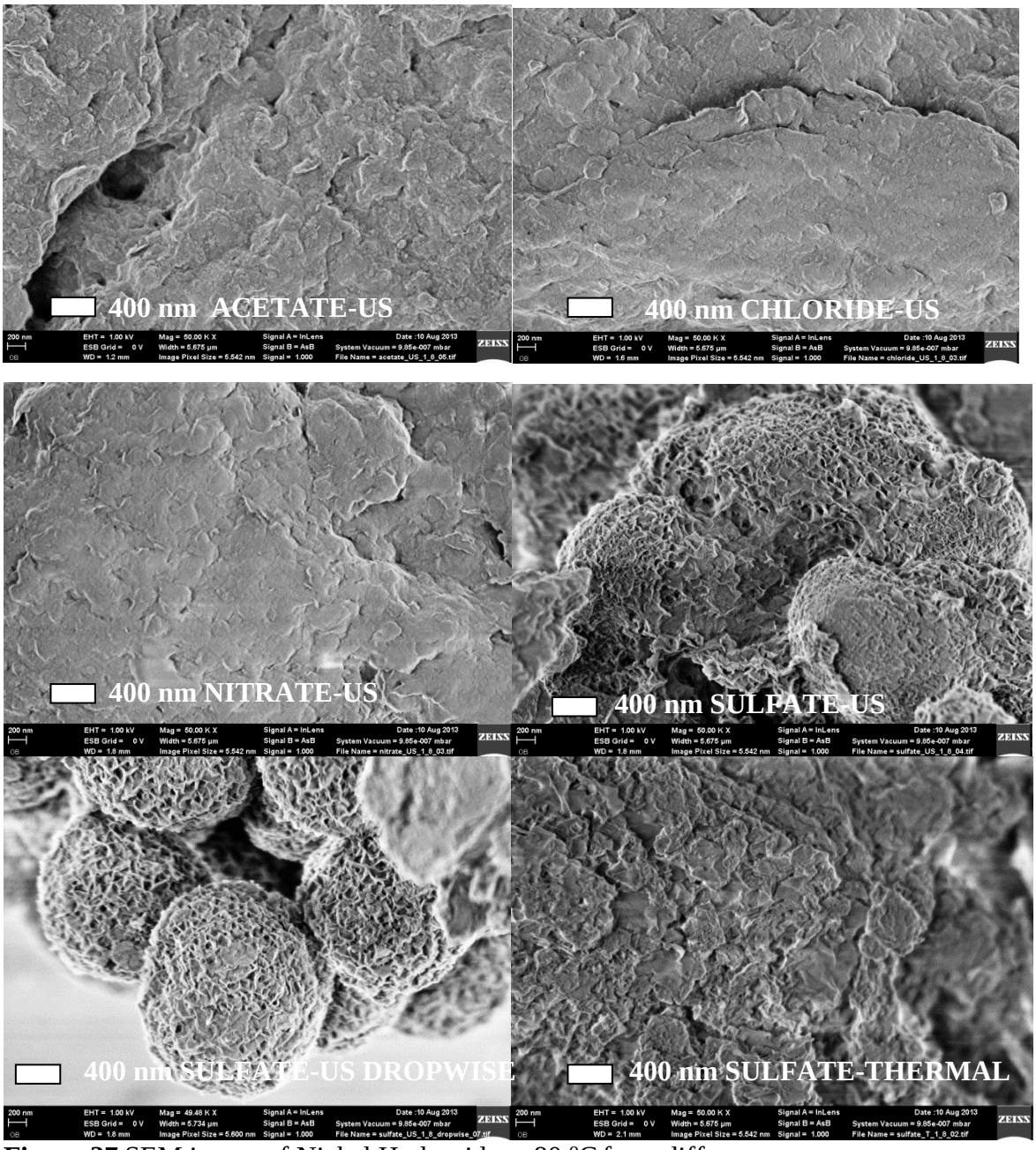

Figure 27 SEM image of Nickel Hydroxide at 80 ^{o}C from different precursors.

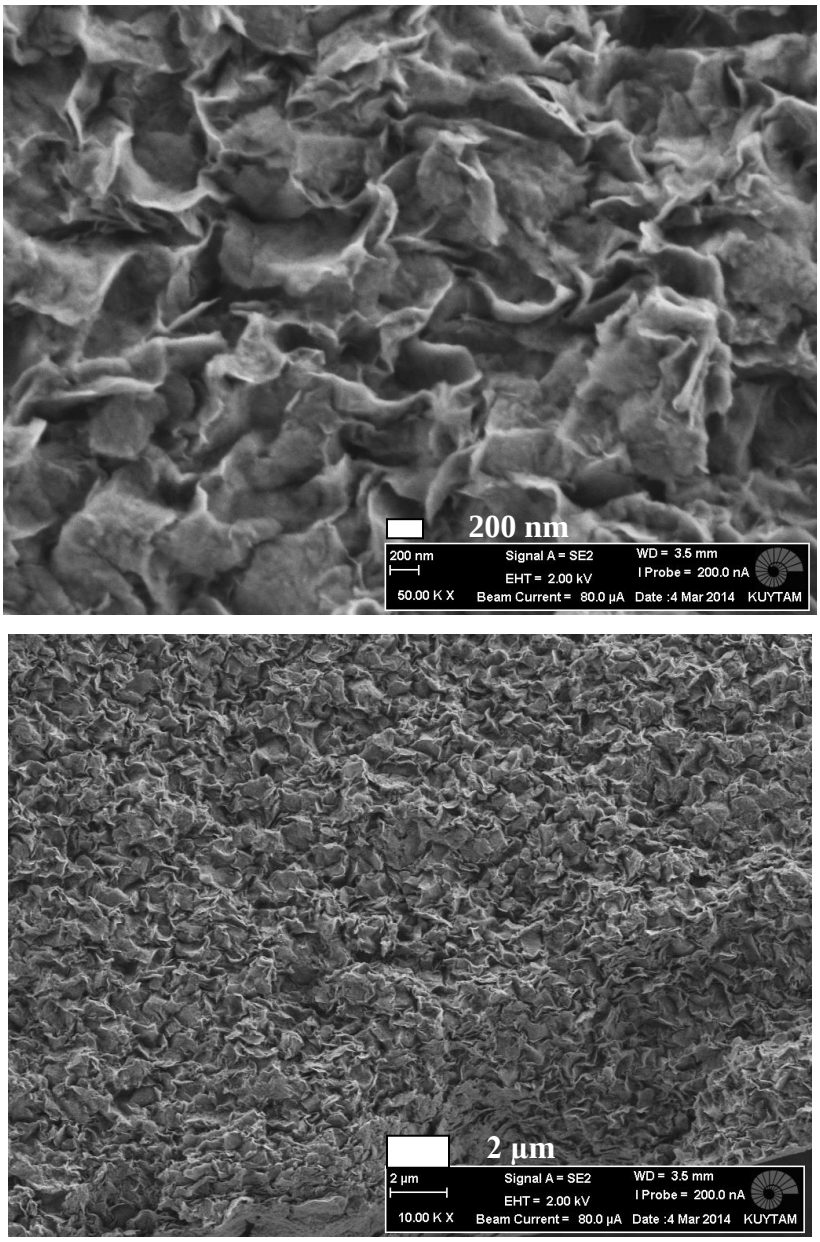

Figure 28 SEM image of Nickel Hydroxide at 100 ^{o}C from acetate precursors.

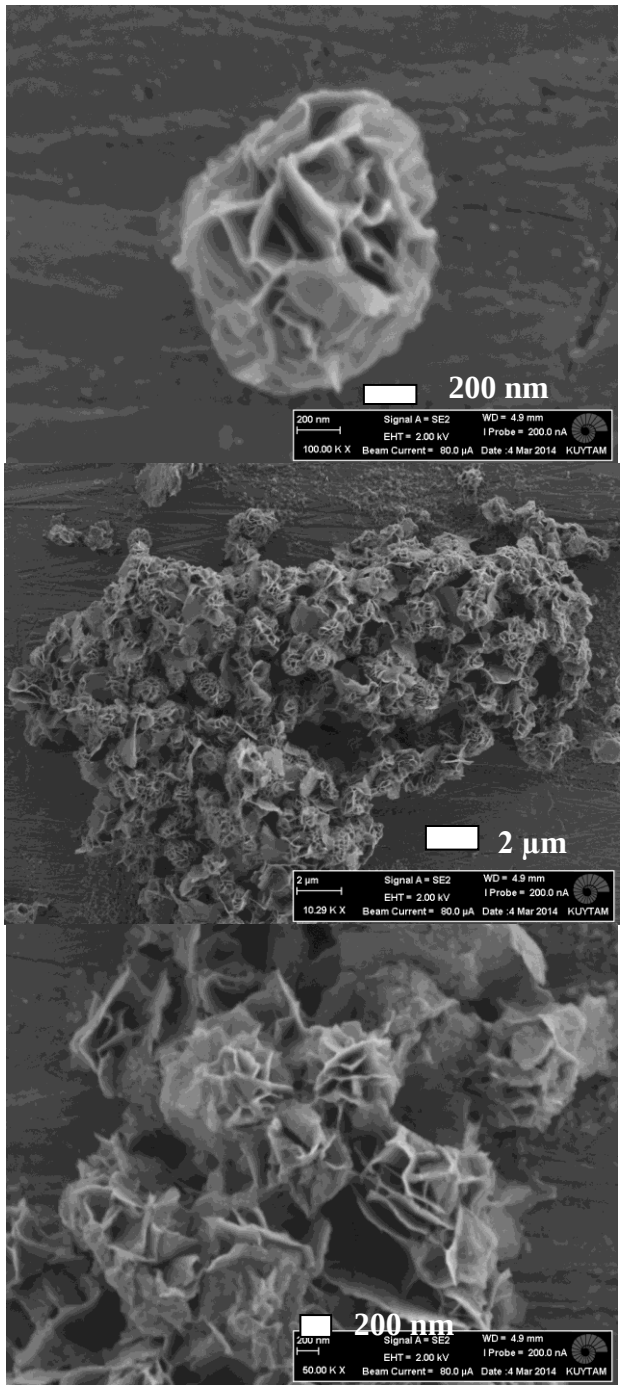

Figure 29 SEM image of Nickel Hydroxide at 100 ^{o}C from acetate precursors with addition of extra acetate anion.

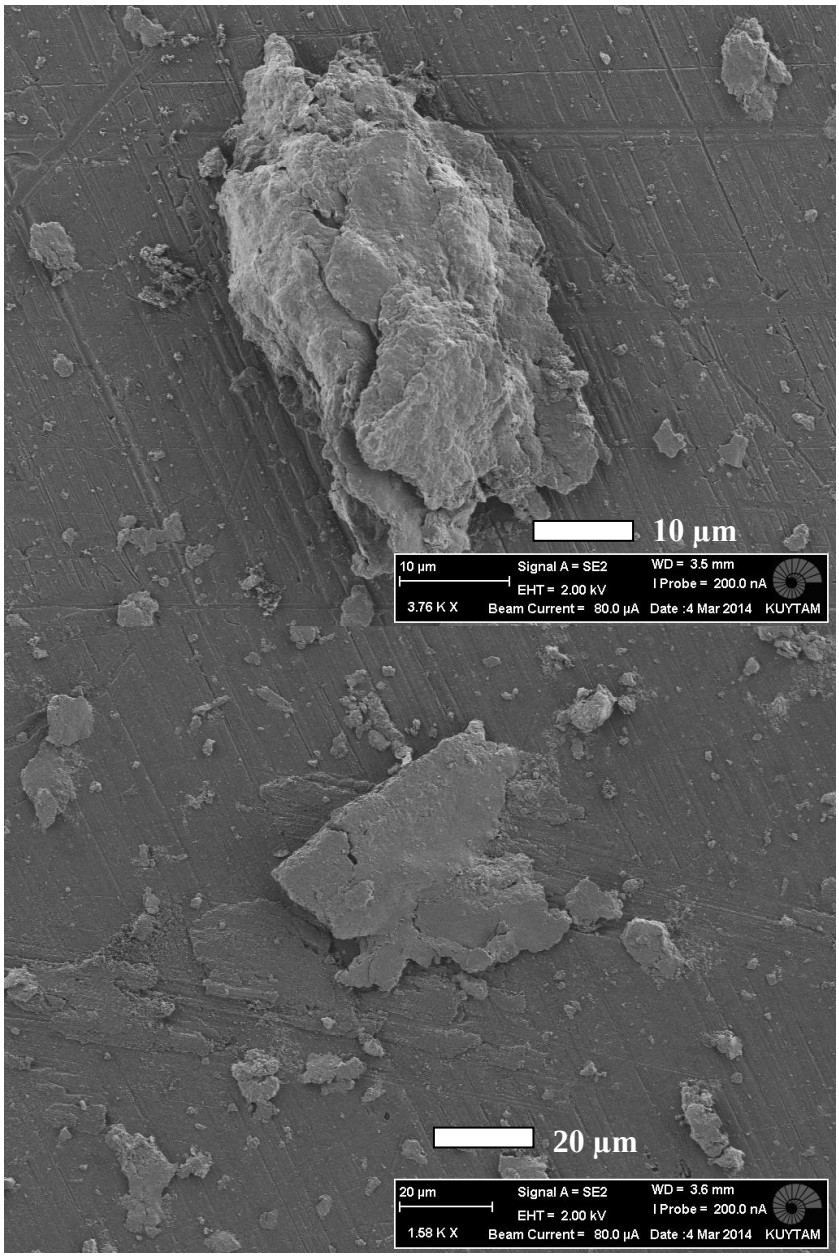

Figure 30 SEM image of Nickel Hydroxide at 100 ºC from chloride precursors.

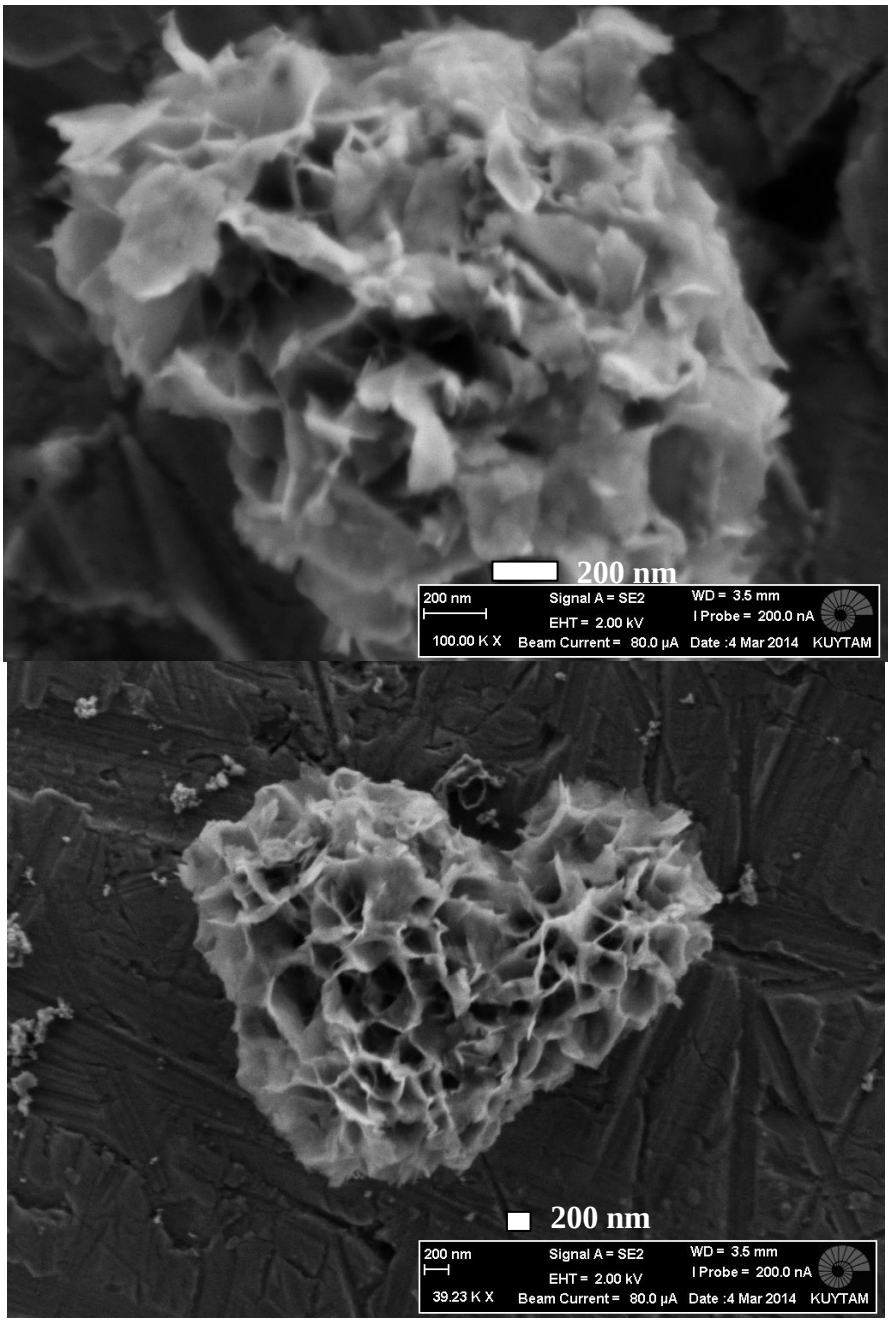

Figure 31 SEM image of Nickel Hydroxide at 100 ºC from chloride precursors with addition of extra chloride anion.

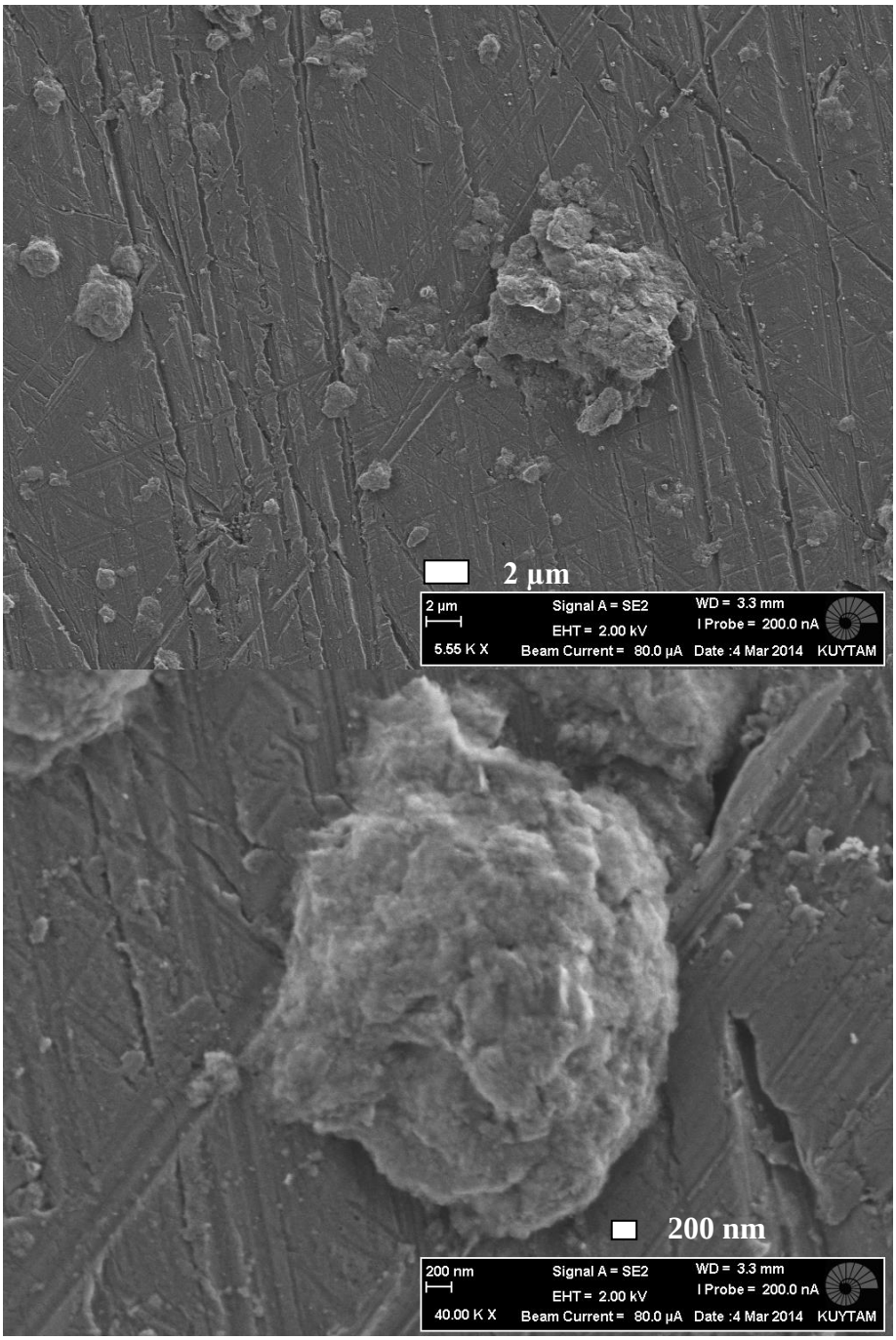

Figure 32 SEM image of Nickel Hydroxide at 100 ºC from nitrate precursors.

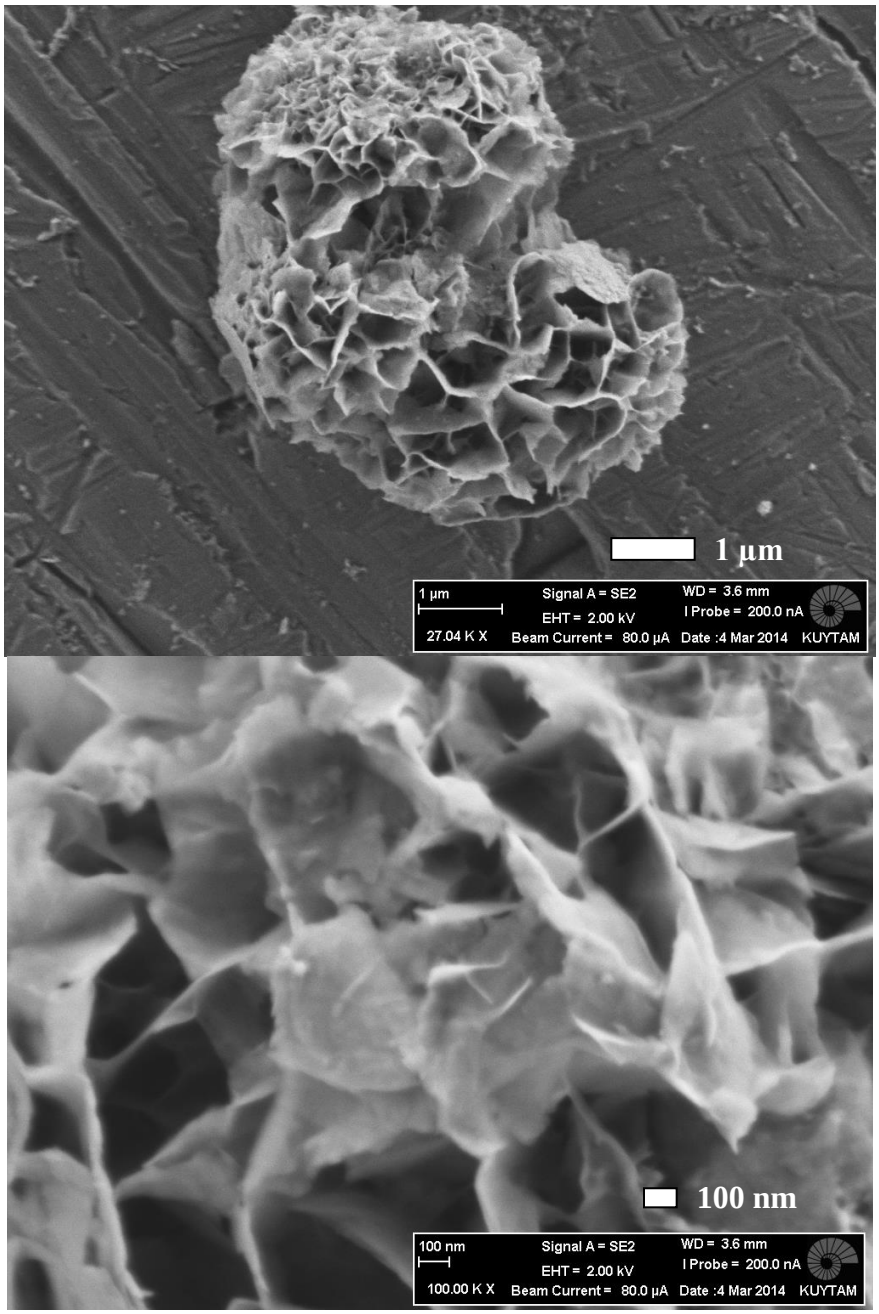

Figure 33 SEM image of Nickel Hydroxide at 100 ^{o}C from nitrate precursors with addition of extra nitrate anion.

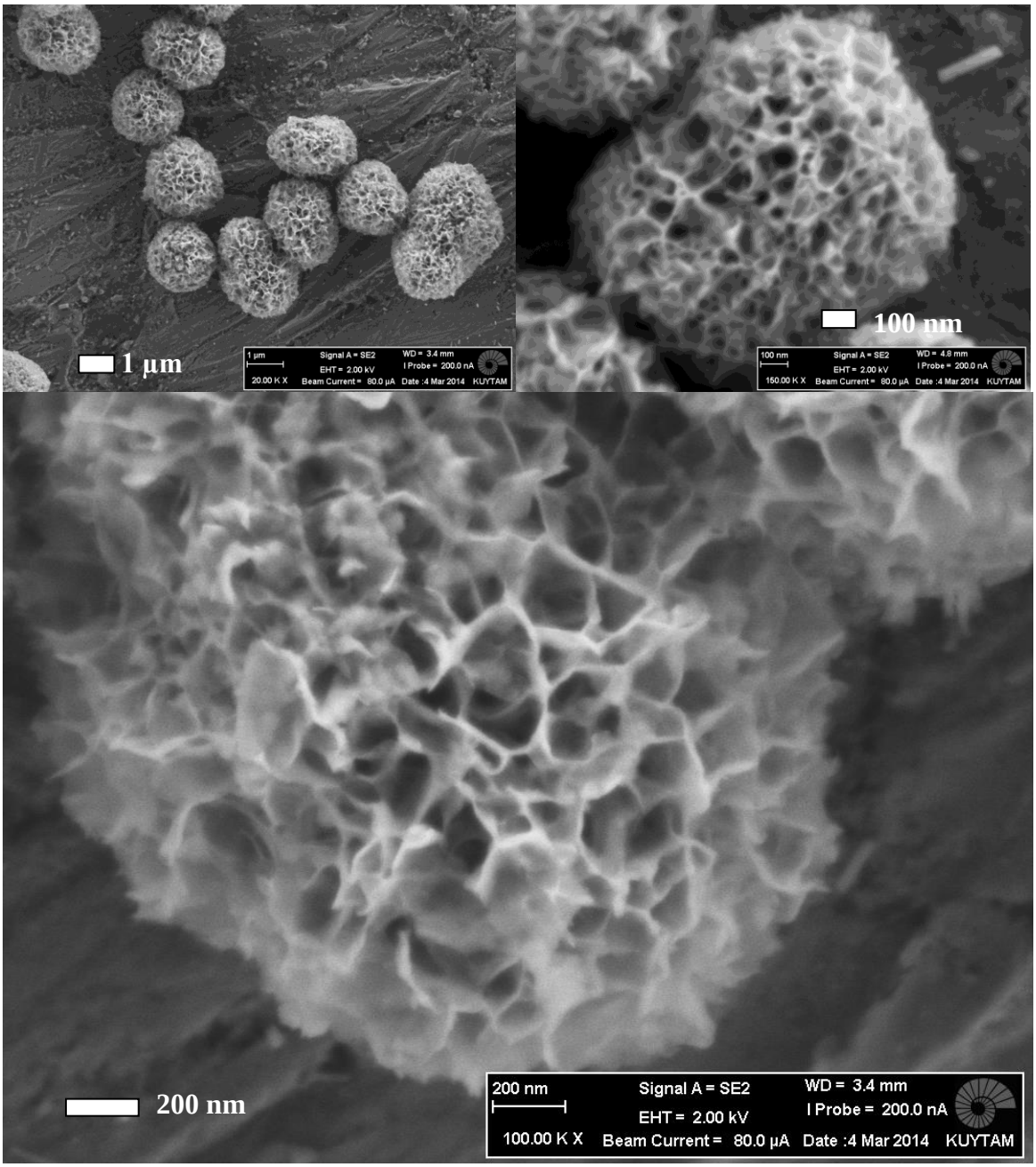

Figure 34 SEM image of Nickel Hydroxide at 100 ^{o}C from sulfate precursors.

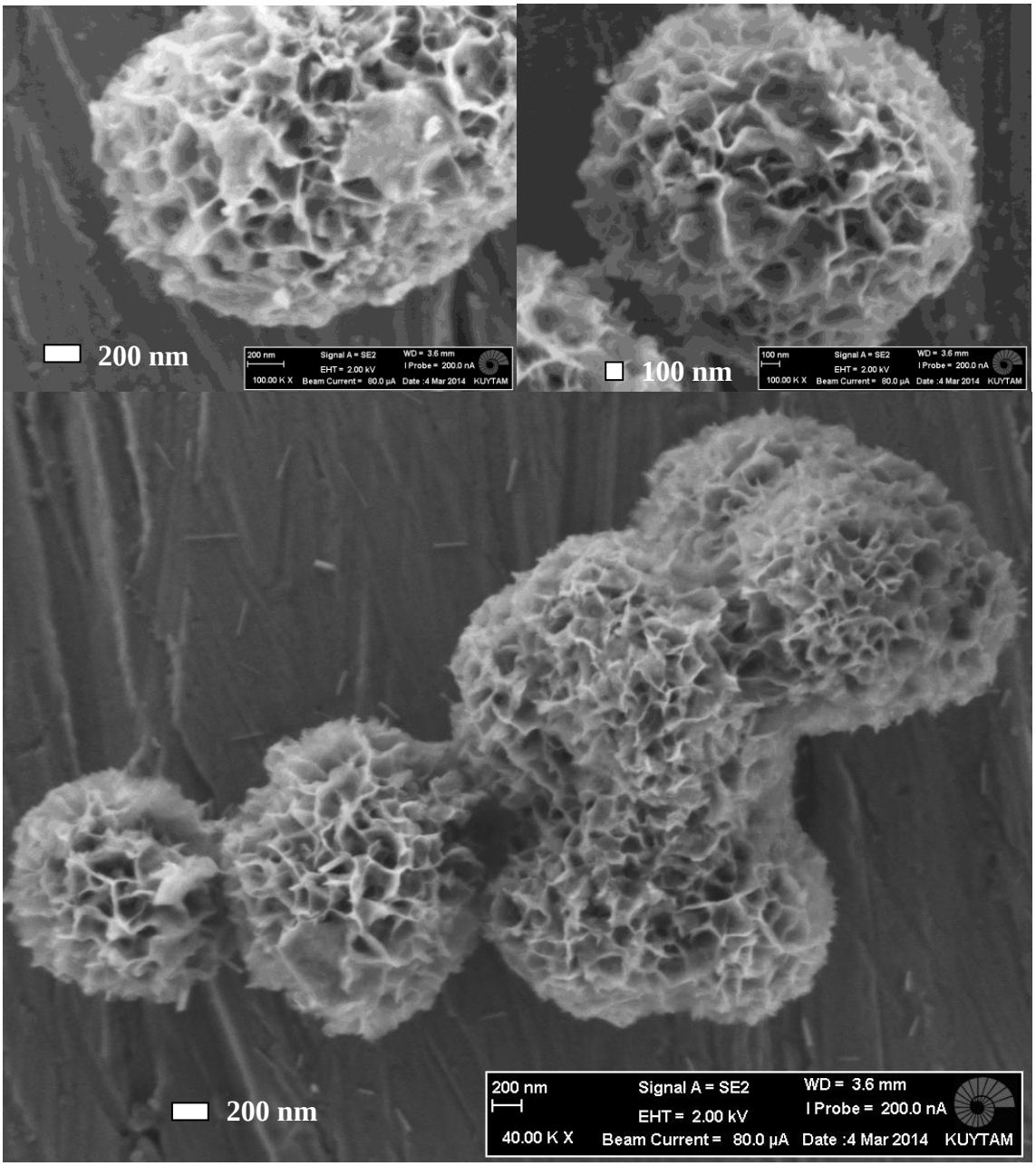

Figure 35 SEM image of Nickel Hydroxide at 100 ^{o}C from sulfate precursors with addition of extra sulfate anion.

Morphological differences with the addition of the extra anion were examined in Figure 28, Figure 29, Figure 30, Figure 31, Figure 32, Figure 33, Figure 34, and Figure 35. Nickel hydroxide synthesized from only sulfate precursor at 100 ^{o}C had sphere flowerlike morphology as seen in Figure 34 shows the SEM images of a typical sample composed of many uniform flowerlike architectures with diameters of 1 μm. A closer observation of the flowerlike nanostructures is shown, which indicated that each flower was composed of dozens of flakelike nanopetals. These nanopetals were connected to each other to build the 3D flowerlike structure.

For acetate precursor, there was sheet flowerlike morphology as seen in Figure 29. After the addition of the extra acetate anion flowerlike sheet spread from each other and formed spherical flowerlike structure.

For chloride (Figure 30) and nitrate (Figure 32) precursors, there was no nanosheet or nanoplate structure before the addition of extra anion. In the initial reaction, irregular morphologies with very thick sheet, only bulk nickel hydroxide particles were seen. They were aggregated structures.

After the addition of the extra anion, the morphology of the nickel hydroxide extremely changed for acetate (Figure 29), nitrate (Figure 33) and chloride (Figure 31) precursors. They had more sphere flowerlike morphology.

3.2.4. Electrochemical Characterization

Electrochemical tests were performed in a three-electrode electrochemical cell at room temperature. Only nickel hydroxides which were prepared from sonication at 100^{o}C were analyzed. Electrodes were prepared from PTFE, carbon black, and nickel hydroxide which were pressed onto nickel foam (1cm^2) as described previously. Prepared electrodes were used as the working electrode, 1cm^2 bare nickel foam was used as the counter electrode, and a Ag/AgCl (sat'd KCl) was used as a reference electrode. The electrolyte solution was 6M KOH aqueous solution. The capacitive properties of nickel hydroxide were characterized by utilizing cyclic voltammetry (CV) and galvanostatic charge-discharge cycling. In CV, electrodes were scanned from -0.2V to 0.6V at 50mV/s scan rate. In charge-discharge cycling, various current densities ranging from 10mA/cm^2 to 100 mA/cm^2 were applied in potential range 0.0-0.5V.

3.2.4.1. Cyclic Voltammetry

Pseudocapacitative properties of electrode materials are generally characterized by specific capacitance C (F/g) which is defined as the charge stored per potential range per mass unit (g). The specific capacitance (SC) can be calculated from the area under the CV curve according to the following equation :

$$C = \frac{1}{mv\Delta V}\int_{V_i}^{V_f} I(V)dV \qquad \textbf{Equation 5}$$

Where m is the mass (g) of the active material, v (V/s) is the scan rate, ΔV (V) is the potential window of scan.

The cyclic voltammograms of synthesized nickel hydroxides from precursors of acetate, chloride, nitrate, and sulfate without additional anion are shown in Figure 36 to Figure 43. All of these hydroxides were scanned for 200 cycles except Sulfate-US-100ºC and Na-Nitrate-US-100ºC. These two electrodes were scanned for 1000 cycles.

During oxidation and reduction in CV measurement, the following reaction take place;

$$\alpha\text{-}Ni(OH)_2 + OH^- \longleftrightarrow \gamma\text{-}NiOOH + H_2O + e^- \qquad (20)$$

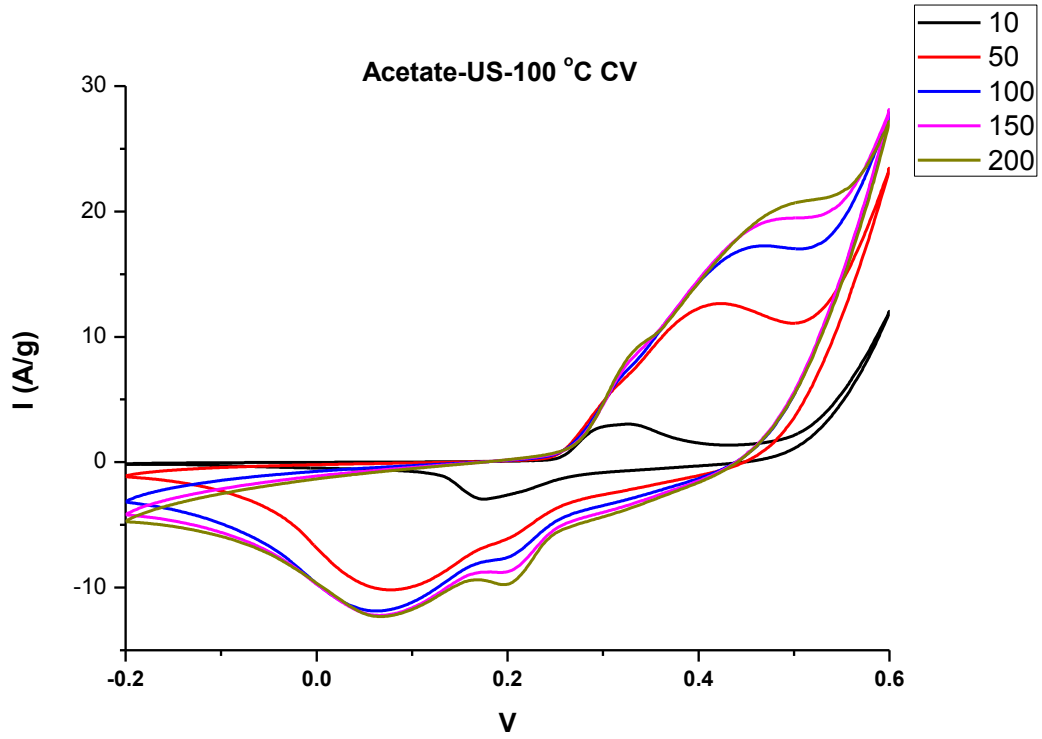

Figure 36 Cyclic voltammograms of $Ni(OH)_2$ at different stages of CV measurement at scan rate of 50 mV/s. The powder was synthesized in presence of acetate precursor.

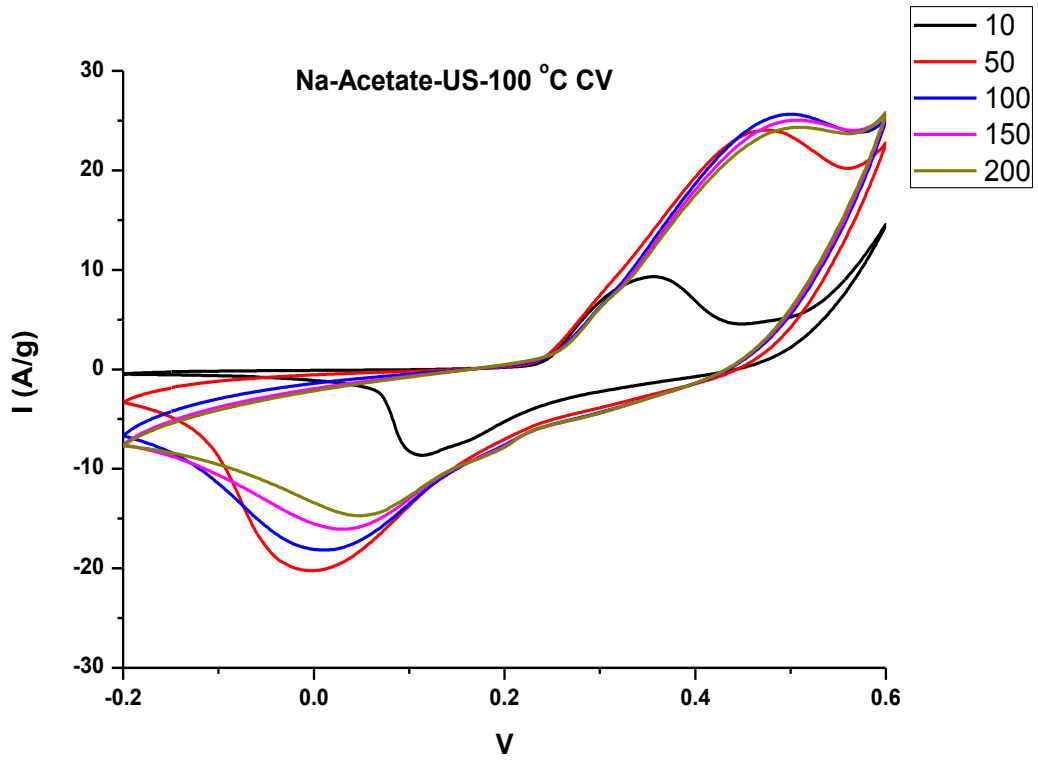

Figure 37 Cyclic voltammograms of $Ni(OH)_2$ at different stages of CV measurement at scan rate of 50mV/s. The powder was synthesized in presence of acetate precursor with addition of extra acetate ion.

Cyclic voltammograms at different cycle numbers of 200 cycle CV measurement for $Ni(OH)_2$ synthesized in presence of acetate precursor without and with addition of extra anion are shown in Figure 36 and Figure 37, respectively. There are two peaks observed during oxidation and reduction corresponding to oxidation of Ni^{2+} to Ni^{3+}, and the reverse process.[21]

The CV shapes for acetate precursor are not consistent like pure α-$Ni(OH)_2$ with the increase of the cycle number and they change with increasing scans. It may be due to the expected ageing of α-phase to β-phase but not known as the exactly the true story. [57] The

anodic and cathodic peak potentials (E_o and E_r respectively) are used to prove the reversibility of the battery. ΔE_o ($E_{oxidation}$-$E_{reduction}$) is a measure of the reversibility of the reaction. $E_{oxidation}$ and $E_{reduction}$ values shift towards from the 1st to 200th scans, confirming the thermodynamic preference for the more stable β-phase. Ironically, ΔE_o also increases with cycling, an indication that the reversibility of the redox transformations decreased.

The $Ni(OH)_2 \leftrightarrow NiOOH$ conversion itself is accompanied by intercalated hydroxyl ions, water, protons, and carbonate and acetate ions. These intercalated ions help chemical ageing in KOH solution and electrochemical ageing between oxidized and reduced states.

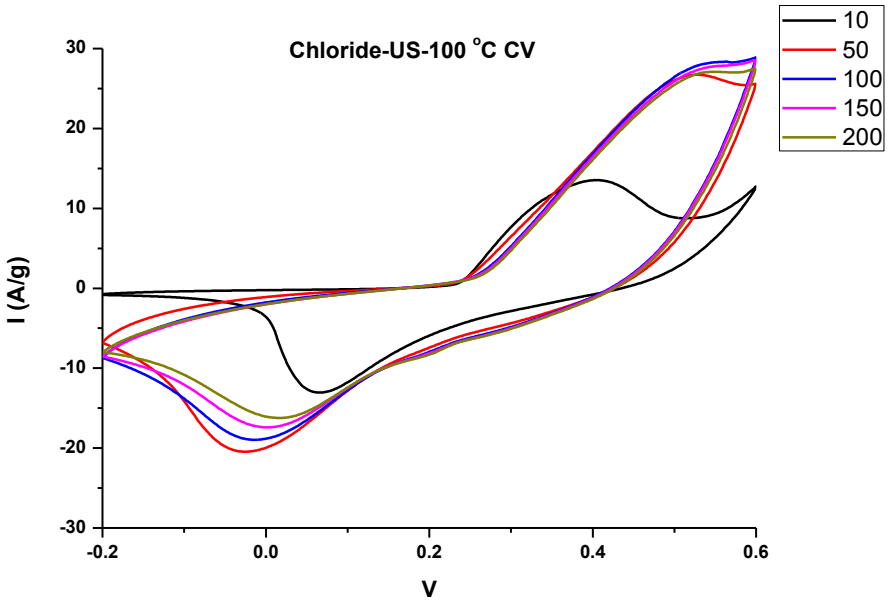

Figure 38 Cyclic voltammograms of $Ni(OH)_2$ at different stages of CV measurement at scan rate of 50mV/s. The powder was synthesized in presence of chloride precursor.

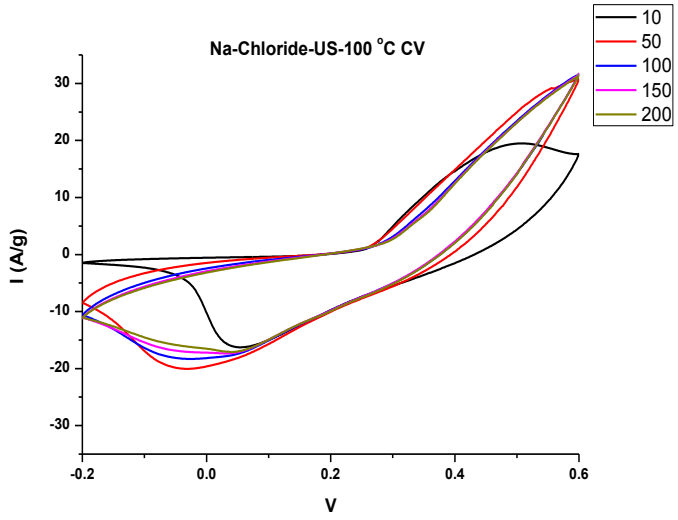

Figure 39 Cyclic voltammograms of $Ni(OH)_2$ at different stages of CV measurement at scan rate of 50mV/s. The powder was synthesized in presence of chloride precursor with addition of extra chloride ion.

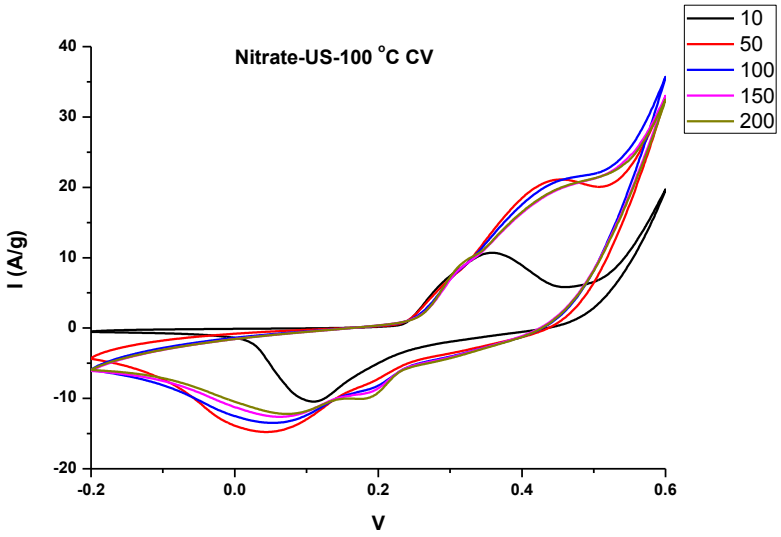

Figure 40 Cyclic voltammograms of $Ni(OH)_2$ at different stages of CV measurement at scan rate of 50mV/s. The powder was synthesized in presence of nitrate precursor.

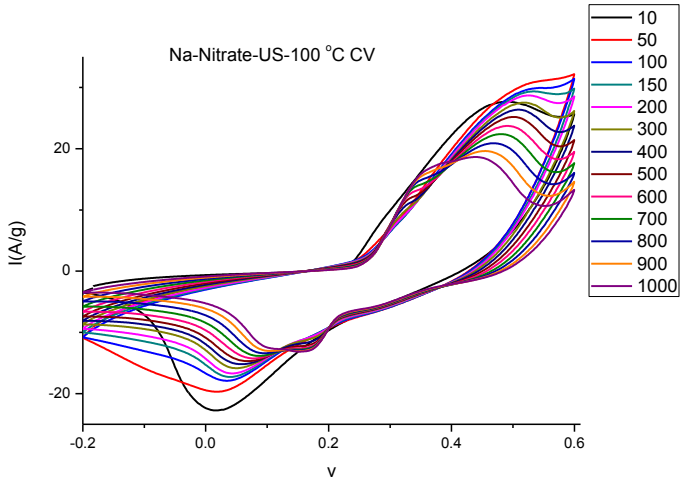

Figure 41 Cyclic voltammograms of $Ni(OH)_2$ at different stages of CV measurement at scan rate of 50mV/s. The powder was synthesized in presence of nitrate precursor with addition of extra nitrate ion.

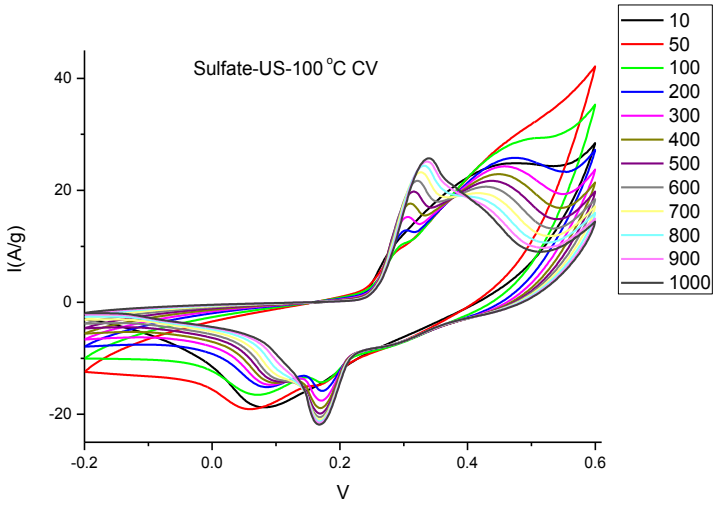

Figure 42 Cyclic voltammograms of $Ni(OH)_2$ at different stages of CV measurement at scan rate of 50mV/s. The powder was synthesized in presence of sulfate precursor.

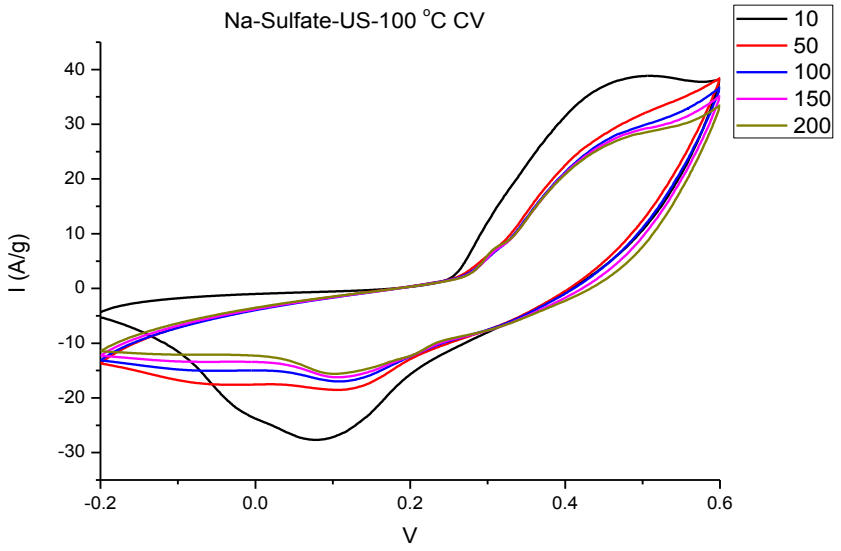

Figure 43 Cyclic voltammograms of $Ni(OH)_2$ at different stages of CV measurement at scan rate of 50mV/s. The powder was synthesized in presence of sulfate precursor with addition of extra sulfate ion.

Table 8 Oxidation and Recduction potential of the samples

	Oxidation Potential(V)	Reduction Potential(V)	ΔV_o *(V)	ΔE**(V)
Ac-02	0.31	0.15	0.16	0.29
NaAc-02	0.36	0.11	0.25	0.24
Cl-02	0.42	0.06	0.36	0.18
NaCl-02	0.43	0.06	0.37	0.17
NO_3-02	0.41	0.07	0.34	0.19
$NaNO_3$-02	0.52	-0.01	0.53	0.08
SO_4-02	0.49	0.03	0.46	0.11
$NaSO_4$-02	0.53	0.03	0.50	0.07

*$\Delta V_o = V_{oxidation} - V_{reduction}$ REVERSIBILITY

** $\Delta E = V_{oxidation\ of\ water} - V_{oxidation}$ CHARGE EFFICIENCY

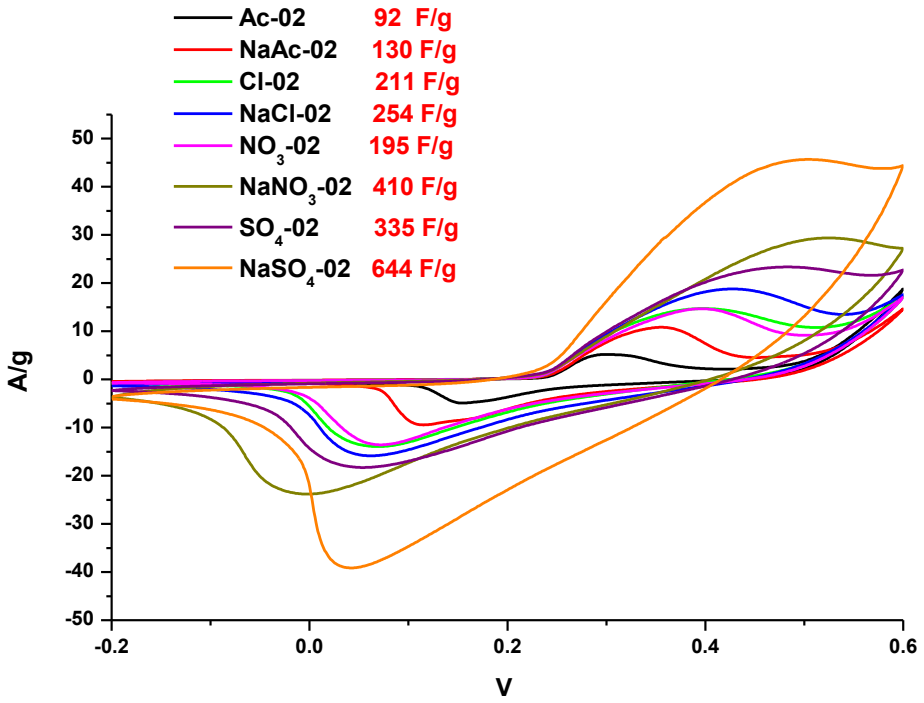

Figure 44 Cyclic voltammograms and corresponding SC values of $Ni(OH)_2$ samples from different precursors with or without addition of the extra ion. CV measurements are performed at a scan rate of 50 mV/s and calculations are made from 10^{th} cycle.

As calculated in Table 8, most reversible sample was found as sulfate precursor synthesized with addition of extra anion as expected. According to charge efficiency acetate showed the best property that was unexpected.

The same phenomenon of acetate precursors is observed for the chloride, nitrate and sulfate precursors. The expected ageing of α-phase to β-phase was occurred with the increase of the cycle number up to 200^{th} cycle of CV. For the measurement done up to 1000 cycle, the ΔE_p values started to decrease and SC started to decrease also after 200^{th} cycle.

Figure 44 represent that adding extra anion increased the area under cyclic voltammogram of the nickel hydroxide for each precursors meaning increase in SC values. It is obvious from the CV diagrams that addition of extra anion enhances electrochemical behavior. The largest area was obtained for the sulfate intercalated samples with additional extra anion. The sequence in decreasing SC is: nitrate, chloride, and acetate.

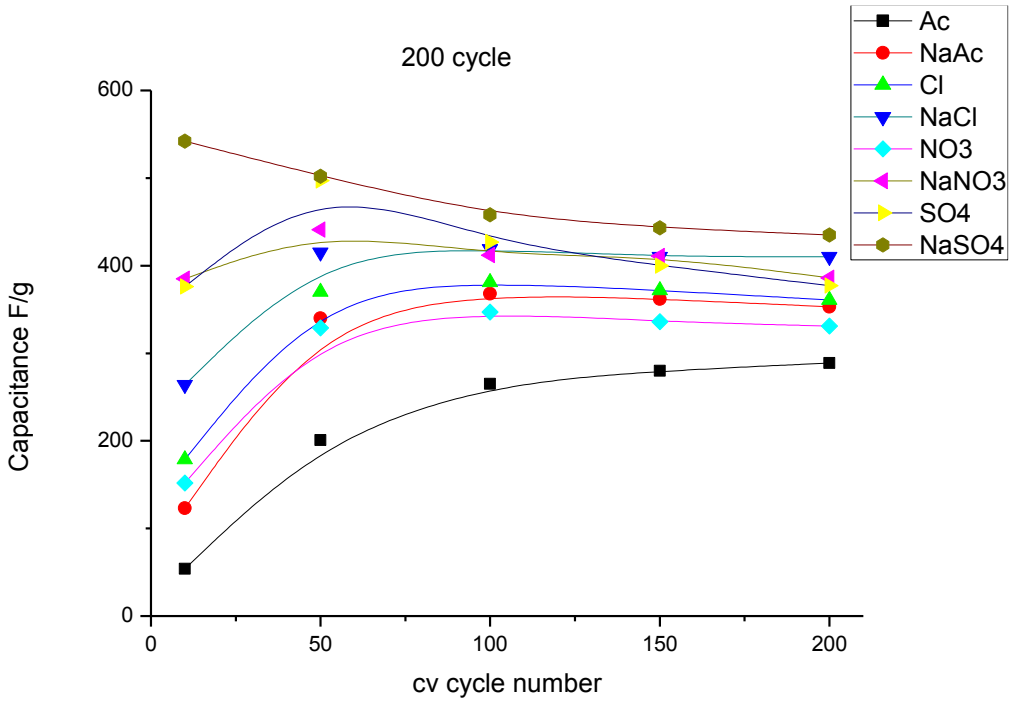

Figure 45 Specific capacitance (F/g) vs cycle number for $Ni(OH)_2$ samples from different precursors and addition of the extra anion. CV measurements are conducted at a scan rate of 50 mV/s.

The increase of SC values with respect to cycle number is also shown in Figure 45. It represents variance of SC with cycle number of CV for nickel hydroxide samples. It was observed that except Na-Sulfate-US-100 ^{o}C precursor the specific capacitances of the nickel hydroxides were increased only up to 50th cycle. Nevertheless, Na-Sulfate-US-100

^{o}C has the highest capacitance after 200 cycles. In all precursors, after 100th cycle specific capacitance values were stabilized.

Specific capacitance values corresponding to different cycles are tabulated in Table 9 and Table 10, and the values are increasing with increasing cycle number. Table 9 represents calculated specific capacitance values (F/g) in different cycles of CV for $Ni(OH)_2$ samples synthesized from different precursors and addition of the extra anion. For sulfate and nitrate precursors, adding extra anion increased the area and specific capacitance almost twice. These results can be attributed to the degree of disturbance in the structure which is influenced by the anion diameter which has order as SO_4^{2-} (516 pm)> Cl^- (368 pm) > NO_3^- (358 pm) >CH_3COO^- (324 pm).[51] Powders prepared from acetate precursors have lowest capacitance among all. Whereas powders synthesized from sulfate ions have the highest capacitance which is in accordance with the previous nickel hydroxide study in the presence of urea as hydroxyl source. [58]

According to Hofmeister Series ability to making the H-bonding of water in bulk solution is decreasing like; sulfate, acetate, chloride, nitrate. [25] Early members of the series called as water structure maker (salting out) increases solvent surface tension, and decrease the solubility of nonpolar molecules. Salting out effect make strength the hydrophobic interaction. By contrast, later salts in the series called as water structure breakers (salting in) increases the solubility of nonpolar molecules and decreases the order in water; in effect, they weaken the hydrophobic effect. According to mechanism Hofmeister series from sulfate to nitrate, ion have affect on the ability to making the H-bonding of water in bulk solution during reaction. Chloride, nitrate and acetate destabilize the system since they have role on the breaking of hydrogen bond of water in bulk solution. Ions which are able to make the H-bonding of water may intercalated more than other ions which are destabilize the system. So the specific capacitances of these precursors are much lower than sulfate precursor.

From the SEM study it was clearly seen that extra anion addition affected the morphology of nickel hydroxide and made the nickel hydroxide porous. So anion exchange becomes easier since the porosity increased the surface area leading to higher diffusion rates in surface of nickel hydroxide.

Table 9 Specific capacitance (F/g) values calculated at different cycle numbers in CV measurement at a scan rate of 50 mV/s 200 cycles.

	Sample ID								
		Acetate US-100 ^{o}C	Na-Acetate US-100 ^{o}C	Chloride US-100 ^{o}C	Na-Chloride US-100 ^{o}C	Nitrate US-100 ^{o}C	Na-Nitrate US-100 ^{o}C	Sulfate US-100 ^{o}C	Na-Sulfate US-100 ^{o}C
Cycle Number	10	54	123	179	264	153	386	376	543
	50	201	340	370	415	330	441	497	503
	100	265	368	381	419	347	413	427	458
	150	280	362	373	410	336	411	401	444
	200	289	353	362	410	332	387	377	436

Table 10 Specific capacitance (F/g) values calculated at different cycle numbers in CV measurement at a scan rate of 50 mV/s 1000 cycles.

		Cycle Number												
Sample ID		10	50	100	150	200	300	400	500	600	700	800	900	1000
	Na-Nitrate US-100 ^{o}C **(F/g)**	386	441	413	411	387	364	340	339	304	288	267	257	233
	Sulfate US-100 ^{o}C **(F/g)**	376	497	427	401	377	342	325	307	296	278	266	259	248

For the 1000 scans of continuous cycling it can be explained that the rationale behind the increase in specific capacitance in the initial 10–50 cycles and then started decreasing up to 1000th cycle. Hydroxyl ion is converted into γ-NiOOH, which leads to an increase in anodic charges, as the γ-phase also is an open structure like α-phase can accommodate easily water molecules or alkali metal cations.[57] With increase in cycling, conversion of α- to β-NiOOH may cause decrease in inter distance so exchange of ions and water may become harder in the material. The conversion of β-NiOOH into γ-NiOOH cannot be taken into consideration in the present study, as it happens only in very high concentrations of alkali. [57]

OH^- ions and protons at the interface between $Ni(OH)_2$ and the KOH electrolyte are responsible for the electron storage mechanism of $Ni(OH)_2$. [59] In the alpha phase of nickel hydroxide, anion coming from the nickel source was also intercalated between nickel hydroxide sheets. It was proved that if the quantity of the intercalated anion increased with the addition of the extra anion, the electron storage could be increased and the SC values of the nickel hydroxide are also increased.

3.2.4.2. Charge/Discharge Performance

Specific capacitance values in charge discharge decrease with increasing current densities as shown in Table 11. The decrease in specific capacitance is attributed to that $Ni(OH)_2$ sheets cannot sustain redox reactions at high current density because of slow transport of charge-compensating OH^- ions in the interlayer galleries. [60]

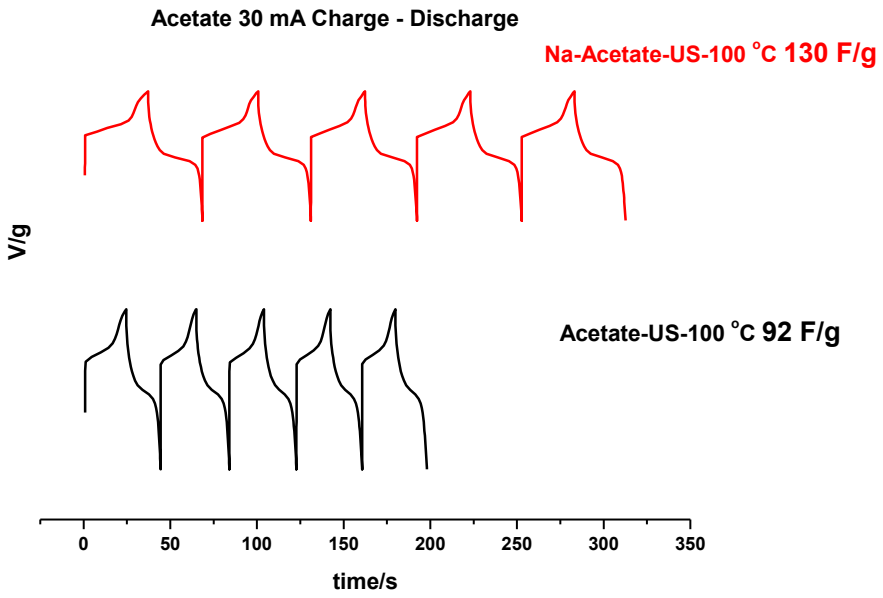

Figure 46 Charge-Discharge curves of $Ni(OH)_2$ prepared from acetate precursor with and without extra anion at current density of 30mA/cm^2.

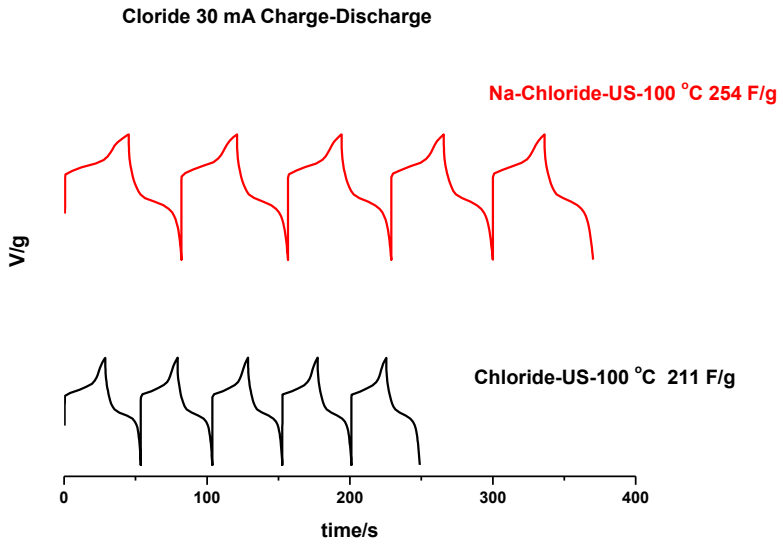

Figure 47 Charge-Discharge curves of $Ni(OH)_2$ prepared from chloride precursor with and without extra anion at current density of $30mA/cm^2$.

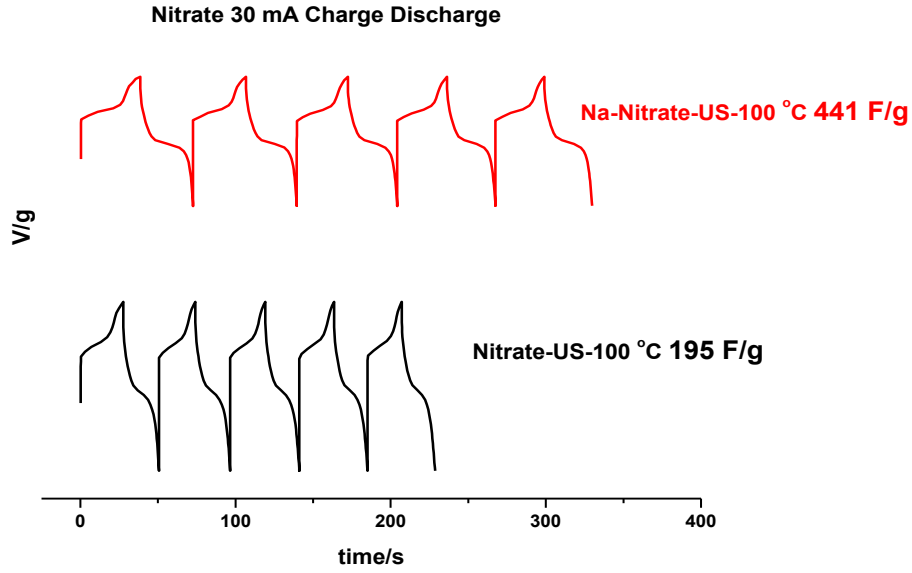

Figure 48 Charge-Discharge curves of $Ni(OH)_2$ prepared from nitrate precursor with and without extra anion at current density of $30mA/cm^2$.

.

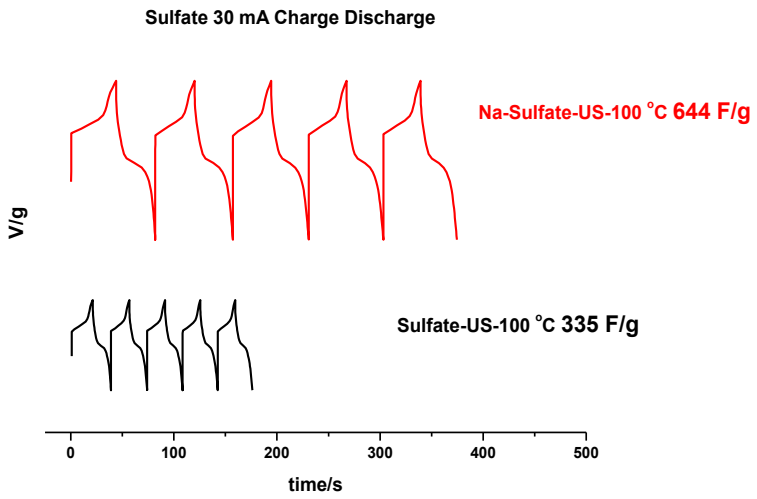

Figure 49 Charge-Discharge curves of $Ni(OH)_2$ prepared from sulfate precursor with and without extra anion at current density of 30 mA/cm^2.

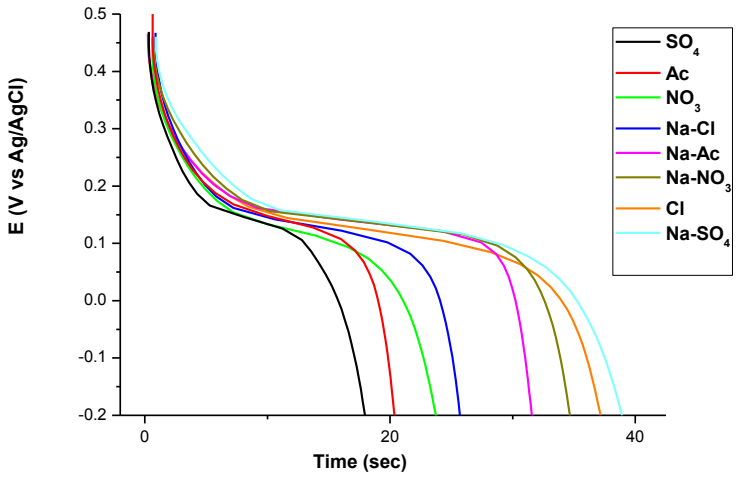

Figure 50 Discharge plots of $Ni(OH)_2$ samples from different precursors and addition of the extra anion measured at current density of 30 mA/cm^2.

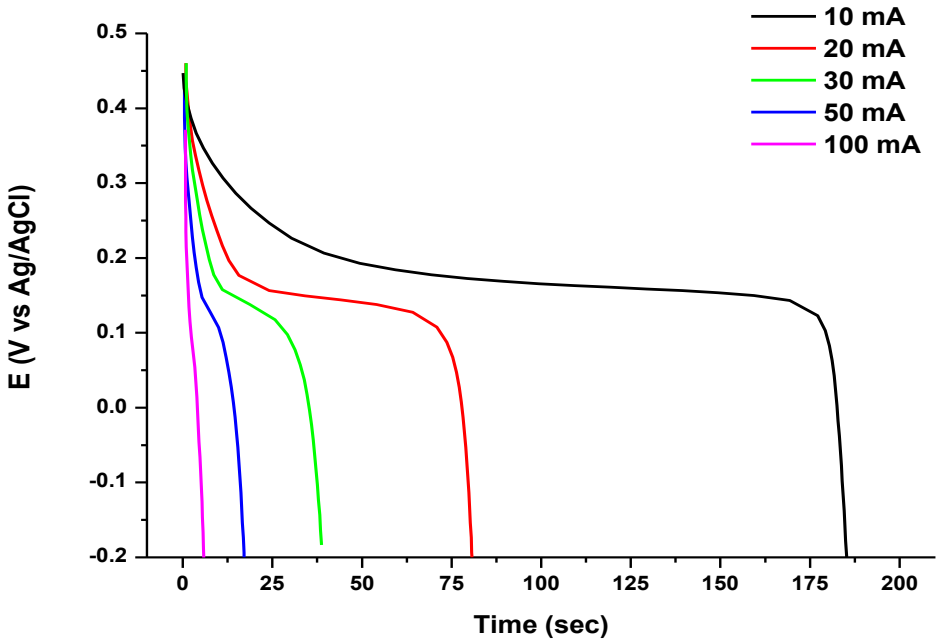

Figure 51 Discharge plots of $Ni(OH)_2$ samples from sulfate precursor with extra anion at different current densities.

Table 11 Specific capacitance values calculated from charge discharge curves for nickel hydroxide prepared from sulfate precursor with extra anion.

Name	Mass (mg)	Current Density (mA/cm^2)	Cycle Number	Charge Time (sec)	Charge Capacitance (F/g)	Discharge Time (sec)	Discharge Capacitance (F/g)	Avg Capacitance (F/g)
Na-SO4-02	**3**	10	1	600.00	2857.14	150.19	715.19	1786.17
Na-SO4-02	**3**	10	2	600.00	2857.14	184.00	**876.19**	
Na-SO4-02	**3**	10	3	600.00	2857.14	129.32	615.81	
Na-SO4-02	**3**	20	1	600.00	5714.29	79.91	761.05	3237.67
Na-SO4-02	**3**	20	2	600.00	5714.29	74.16	**706.29**	3210.29
Na-SO4-02	**3**	20	3	98.90	941.90	71.55	681.43	811.67
Na-SO4-02	**3**	20	4	80.77	769.24	68.92	656.38	712.81
Na-SO4-02	**3**	20	5	77.55	738.57	98.02	933.52	836.05
Na-SO4-02	**3**	30	1	43.48	621.14	38.08	544.00	582.57
Na-SO4-02	**3**	30	2	38.13	544.71	37.08	**529.71**	537.21
Na-SO4-02	**3**	30	3	37.04	529.14	36.61	523.00	526.07
Na-SO4-02	**3**	30	4	36.65	523.57	35.78	511.14	517.36
Na-SO4-02	**3**	30	5	36.08	515.43	35.23	503.29	509.36
Na-SO4-02	**3**	50	1	19.82	471.90	16.56	394.29	433.10
Na-SO4-02	**3**	50	2	16.61	395.48	16.42	**390.95**	393.21
Na-SO4-02	**3**	50	3	16.39	390.24	16.31	388.33	389.29
Na-SO4-02	**3**	50	4	16.29	387.86	16.21	385.95	386.90
Na-SO4-02	**3**	50	5	16.19	385.48	16.11	383.57	384.52
Na-SO4-02	**3**	100	1	6.92	329.52	5.09	242.38	285.95
Na-SO4-02	**3**	100	2	5.11	243.33	5.10	**242.86**	243.10
Na-SO4-02	**3**	100	3	5.07	241.43	5.08	241.90	241.67
Na-SO4-02	**3**	100	4	5.06	240.95	5.07	241.43	241.19
Na-SO4-02	**3**	100	5	5.05	240.48	5.05	240.48	240.48

Table 12 Specific capacitance values calculated from charge discharge plots for $Ni(OH)_2$ samples from different precursors and addition of the extra anion measured at current density of 30 mA/cm^2.

Name	Mass (mg)	Current (mA)	Cycle Number	Charge Time (sec)	Charge Capacitance (F/g)	Discharge Time (sec)	Discharge Capacitance (F/g)	Avg Capacitance (F/g)
Ac-02	**4.2**	30	1	23.47	239.49	19.720	201.22	220.36
Ac-02	**4.2**	30	2	20.62	210.41	19.130	195.20	202.81
Ac-02	**4.2**	30	3	19.91	203.16	18.73	191.12	197.14
Ac-02	**4.2**	30	4	19.46	198.57	18.43	188.06	193.32
Ac-02	**4.2**	30	5	19.13	195.20	17.99	183.57	189.39
Na-Ac-02	**5.2**	30	1	36.42	300.16	31.32	258.13	279.15
Na-Ac-02	**5.2**	30	2	32.14	264.89	30.43	250.80	257.84
Na-Ac-02	**5.2**	30	3	31.24	257.47	29.97	247.01	252.24
Na-Ac-02	**5.2**	30	4	30.77	253.60	29.65	244.37	248.98
Na-Ac-02	**5.2**	30	5	30.44	250.88	29.38	242.14	246.51
Cl-02	**4.7**	30	1	44.46	405.41	36.87	336.20	370.81
Cl-02	**4.7**	30	2	38.92	354.89	35.58	324.44	339.67
Cl-02	**4.7**	30	3	37.54	342.31	34.79	317.23	329.77
Cl-02	**4.7**	30	4	36.74	335.02	34.29	312.67	323.84
Cl-02	**4.7**	30	5	35.31	321.98	33.96	309.67	315.82
Na-Cl-02	**5.5**	30	1	28.44	221.61	44.83	193.48	207.55
Na-Cl-02	**5.5**	30	2	25.69	200.18	44.32	189.51	194.84
Na-Cl-02	**5.5**	30	3	25.10	195.58	43.94	186.55	191.06
Na-Cl-02	**5.5**	30	4	24.66	192.16	43.68	184.52	188.34
Na-Cl-02	**5.5**	30	5	24.31	189.43	43.47	182.88	186.16

Table 13 Specific capacitance values calculated from charge discharge plots for $Ni(OH)_2$ samples from different precursors and addition of the extra anion measured at current density of 30 mA/cm^2.

Name	Mass (mg)	Current (mA)	Cycle Number	Charge Time (sec)	Charge Capacitance (F/g)	Discharge Time (sec)	Discharge Capacitance (F/g)	Avg Capacitance (F/g)
NO_3-02	**4.2**	30	1	27.25	278.06	23.13	236.02	257.04
NO_3-02	**4.2**	30	2	23.42	238.98	22.36	228.16	233.57
NO_3-02	**4.2**	30	3	22.71	231.73	21.38	218.16	224.95
NO_3-02	**4.2**	30	4	22.31	227.65	21.65	220.92	224.29
NO_3-02	**4.2**	30	5	22.03	224.80	21.44	218.78	221.79
Na-NO_3-02	**5.5**	30	1	38.13	297.12	34.01	265.01	281.06
Na-NO_3-02	**5.5**	30	2	34.15	266.10	32.69	254.73	260.42
Na-NO_3-02	**5.5**	30	3	32.89	256.29	31.82	247.95	252.12
Na-NO_3-02	**5.5**	30	4	32.02	249.51	31.21	243.19	246.35
Na-NO_3-02	**5.5**	30	5	31.51	245.53	30.61	238.52	242.03
SO_4-02	**5.3**	30	1	20.41	165.04	17.67	142.88	153.96
SO_4-02	**5.3**	30	2	17.97	145.31	17.33	140.13	142.72
SO_4-02	**5.3**	30	3	17.45	141.11	17.33	140.13	140.62
SO_4-02	**5.3**	30	4	17.22	139.25	16.63	134.47	136.86
SO_4-02	**5.3**	30	5	16.83	136.09	16.63	134.47	135.28
Na-SO_4-02	**3**	30	1	43.48	621.14	38.08	544.00	582.57
Na-SO_4-02	**3**	30	2	38.13	544.71	37.08	529.71	537.21
Na-SO_4-02	**3**	30	3	37.04	529.14	36.61	523.00	526.07
Na-SO_4-02	**3**	30	4	36.65	523.57	35.78	511.14	517.36
Na-SO_4-02	**3**	30	5	36.08	515.43	35.23	503.29	509.36

Specific capacitance was calculated;

$$C = \frac{I}{(\Delta E / \Delta t) \times m}$$ **Equation 6**

Where I is the constant discharging current, $\Delta E/\Delta t$ indicates the slope of the discharge plot of the discharging curves, and m is the mass of the active electrode material.

From Table 11 it is observed that sequence of decreasing SC is: sulfate, nitrate, chloride, and acetate which indicates that sulfate intercalated $Ni(OH)_2$ had the highest capacitance among the samples studied. The extra anion affected the capacitance positively and capacitance increased in each precursors.

With increasing current density, the specific capacitance decreases gradually in Figure 51, which can be attributed to electrolytic ions diffusing and migrating into the active materials slower at higher current densities. At high current densities, the diffusion effect limits the migration of the electrolytic ions, causes active surface areas to become inaccessible for charge storage. We also observe that the specific capacitance of the $Ni(OH)_2$ samples decreases from 876 to 242 F/g as the current increases to 100 mA/cm^2, representing only a 28% decrease compared with the specific capacitance at a current density of 10 mA/cm^2.

In Wu and Huang study, published on *International Journal of Hydrogen Energy* article in 2007, specific capacitance of the deposited electrode is 167.3 F/g at 1 A/g charge/discharge, and 156.6 F/g at 16.5 A/g which were lower than our study. [61]

In Li and Yang study, published on *Nature Communications* in 2013, the specific capacitances of the amorphous $Ni(OH)_2$ samples were calculated to be 2,188, 1,943, 1,667, 1,484, 1,367 and 1,250 F/g at scan rates of 1, 2, 5, 10, 15 and 20 mV/s .[62] Even the amorphous nickel hydroxide had higher specific capacitance then our material; they did not

perform any endurance test of sample which shows the degradation of the specific capacitance.

From the comparison with literature values for specific capacitances of nickel hydroxides, it can be said that produced samples have comparable capacitance values. First, α-$Ni(OH)_2$ has superior electrochemical properties relative to β-$Ni(OH)_2$. The second is the unique morphology of α-$Ni(OH)_2$ which provides feasible access of OH^- ions and water to the $Ni(OH)_2$ edge planes and thus to the interlayer galleries. To date, electroactive materials with hierarchical morphologies based on layered structures have generally shown higher specific capacitance relative to bulk-type materials. [63] Therefore, extra addition ion played a crucial role in achieving higher specific capacitances.

Chapter 4

4. Conclusion

Alpha-Nickel Hyrdoxide was synthesized by the sonochemical degradation of OH^- sources urea and hexamethyl tetramine. Firstly it was proved that ultrasound yielded products with properties significantly different than the products obtained by thermal degradation of OH^- sources. Secondly the effect of intercalating chloride, nitrate, acetate, and sulfate anions on morphology and electrochemical performance was studied. Sulfate precursors had the highest specific capacitance over all other precursors. The specific capacitance trend also differed from the literature values, and the value for the sulfate-intercalated sample was larger than that of acetate- and nitrate intercalated samples. Ultrasonic synthesis increased the specific capacitance of the sulfate-intercalated sample significantly. This sample was also the most reversible and had the highest charge efficiency.

For the hexamethyl tetramine decomposition; electrochemical performance was increased with respect to urea decomposition since cyanate ion that is byproduct of the urea decomposition decrease the electrochemical performance. Specific capacitance of the nickel hydroxide was increased up to 50% for sulfate precursor. It was also examined that adding extra anion whether increase the electrochemical properties or not in this study. It was proved that adding extra anion increased the electrochemical performance 90% for sulfate precursor. It was also proved morphologically that adding extra anion made nickel hydroxide more crystallite. Among the all precursors only sulfate precursor has porous flower structure according to SEM images for 80 ^oC. For charge discharge analysis sulfate precursor synthesized with addition of extra anion showed best properties among all.

Chapter 5

5. Bibliography

1. Mason, T. J. a. J. P. L., *Sonochemistry: theory, applications and uses of ultrasound in chemistry*. Ellis Horwood, 1988.
2. Hart, C. G. a. D. P., Ultrasound Induced Cavitation and Sonochemical Yields. *Journal of the Acoustical Society of America* **1998,** *Vol. 104*.
3. Suslick, K. S.; Hammerton, D. A.; Cline, R. E., Sonochemical hot spot. *Journal of the American Chemical Society* **1986,** *108* (18), 5641-5642.
4. Thompson, L. H.; Doraiswamy, L. K., Sonochemistry: Science and Engineering. *Industrial & Engineering Chemistry Research* **1999,** *38* (4), 1215-1249.
5. Suslick, K. S., Sonochemistry. Review article. **1990**.
6. Frederick, J. R., Ultrasonic Engineering. *John Wiley & Sons, New York, 1965*, , 116-164.
7. Kaş R. , B. Ö., Sonochemical shape control of copper hydroxysulfates. *Ultrasonics Sonochemistry* **2012,** *19*, 692-700

8. Okitsu, K.; Sharyo, K.; Nishimura, R., One-Pot Synthesis of Gold Nanorods by Ultrasonic Irradiation: The Effect of pH on the Shape of the Gold Nanorods and Nanoparticles. *Langmuir* **2009,** *25* (14), 7786-7790.
9. Wahab, R.; Ansari, S. G.; Kim, Y.-S.; Seo, H.-K.; Shin, H.-S., Room temperature synthesis of needle-shaped ZnO nanorods via sonochemical method. *Applied Surface Science* **2007,** *253* (18), 7622-7626.
10. Weidner, V. S. a. J. W., An Electrochemical Route for Making Porous Nickel Oxide Electrochemical Capacitors. ,*J. Electrochem. Society* **1997,**
144(8).
11. Anderson, K. C. L. a. M. A., Porous Nickel Oxide/Nickel Films for Electrochemical Capacitors
J. Electrochem. Society **1996** *143(1)*, 124-130.
12. Kim, K.-W. N. a. K.-B., A Study of the Preparation of NiOx Electrode via Electrochemical Route for Supercapacitor Applications and Their Charge Storage Mechanism
J. Electrochemical Society **2002,** *149(3)*, 346-354.
13. Srinivasan, V.; Weidner, J. W., Capacitance studies of cobalt oxide films formed via electrochemical precipitation. *Journal of Power Sources* **2002,** *108* (1–2), 15-20.

14. Suh-Cem Panga, M. A. A. a. T. W. C., Novel Electrode Materials for Thin-Film Ultracapacitors: Comparison of Electrochemical Properties of Sol-Gel-Derived and Electrodeposited Manganese Dioxide
J. Electrochem. Society **2000,** *147*.
15. Wang, S. Y.; Wu, N. L., Operating characteristics of aqueous magnetite electrochemical capacitors. *Journal of Applied Electrochemistry* **2003,** *33* (3-4), 345-348.
16. D. Linden, M. G. H., *Handbook of Batteries*. New York, 1995.
17. Dhar, S. K.; Ovshínsky, S. R.; Gifford, P. R.; Corrigan, D. A.; Fetcenko, M. A.; Venkatesan, S., Nickel/metal hydride technology for consumer and electric vehicle batteries—a review and up-date. *Journal of Power Sources* **1997,** *65* (1–2), 1-7.
18. Doyle, R. L.; Godwin, I. J.; Brandon, M. P.; Lyons, M. E. G., Redox and electrochemical water splitting catalytic properties of hydrated metal oxide modified electrodes. *Physical Chemistry Chemical Physics* **2013,** *15* (33), 13737-13783.
19. Faure, C., Delmas, C. ,Fouassier, M., Characterization of a turbostratic α-nickel hydroxide quantitatively obtained from an nickel sulfate solution
J. Power Sources **1991,** *35 (3)*, 279-90.
20. Hall, D. S.; Lockwood, D. J.; Poirier, S.; Bock, C.; MacDougall, B. R., Raman and Infrared Spectroscopy of α and β Phases of Thin Nickel Hydroxide Films Electrochemically Formed on Nickel. *The Journal of Physical Chemistry A* **2012,** *116* (25), 6771-6784.
21. Lee, J. W.; Ko, J. M.; Kim, J.-D., Hierarchical Microspheres Based on α-Ni(OH)2 Nanosheets Intercalated with Different Anions: Synthesis, Anion Exchange, and Effect of Intercalated Anions on Electrochemical Capacitance. *The Journal of Physical Chemistry C* **2011,** *115* (39), 19445-19454.
22. Hu, W.-K.; Noréus, D., Alpha Nickel Hydroxides as Lightweight Nickel Electrode Materials for Alkaline Rechargeable Cells. *Chemistry of Materials* **2003,** *15* (4), 974-978.
23. Li, H.; Ma, J.; Evans, D. G.; Zhou, T.; Li, F.; Duan, X., Molecular Dynamics Modeling of the Structures and Binding Energies of α-Nickel Hydroxides and Nickel−Aluminum Layered Double Hydroxides Containing Various Interlayer Guest Anions. *Chemistry of Materials* **2006,** *18* (18), 4405-4414.
24. F.Hofmeister Arch. Exp. Pathol. Pharmacol. 24, -.
25. Hofmeister, F., Arch. Exp. Pathol. Pharmakol. 1888; Vol. 24, pp 247-260.
26. Portemer, F., Delahaye-Vidal, A. and Figlarz, M., , Characterization of active material deposited at the nickel hydroxide electrode by electrochemical impregnation. . *Journal of the Electrochemical Society* **1992,** *139(3)*.
27. Kamath, P. V. a. S., G. N. , , Electroless nickel hydroxide: synthesis and characterization. *Journal of Applied Electrochemistry* **1992,** *22*.

28. Ramesh, T. N.; Kamath, P. V., Synthesis of nickel hydroxide: Effect of precipitation conditions on phase selectivity and structural disorder. *Journal of Power Sources* **2006,** *156* (2), 655-661.
29. Soler-Illia, G. J. d. A. A.; Jobbágy, M.; Regazzoni, A. E.; Blesa, M. A., Synthesis of Nickel Hydroxide by Homogeneous Alkalinization. Precipitation Mechanism. *Chemistry of Materials* **1999,** *11* (11), 3140-3146.
30. Akinc, M.; Jongen, N.; Lemaître, J.; Hofmann, H., Synthesis of nickel hydroxide powders by urea decomposition. *Journal of the European Ceramic Society* **1998,** *18* (11), 1559-1564.
31. Avena, M. J.; Vazquez, M. V.; Carbonio, R. E.; Pauli, C. P.; Macagno, V. A., A simple and novel method for preparing Ni(OH)2 Part I: Structural studies and voltammetric response. *Journal of Applied Electrochemistry* **1994,** *24* (3), 256-260.
32. Coudun, C.; Amblard, E.; Guihaumé, J.; Hochepied, J.-F., Nanostructured particles by controlled precipitation techniques: Example of nickel and cobalt hydroxides. *Catalysis Today* **2007,** *124* (1–2), 49-54.
33. Yang, D.; Wang, R.; He, M.; Zhang, J.; Liu, Z., Ribbon- and Boardlike Nanostructures of Nickel Hydroxide: Synthesis, Characterization, and Electrochemical Properties. *The Journal of Physical Chemistry B* **2005,** *109* (16), 7654-7658.
34. Cao, M.; He, X.; Chen, J.; Hu, C., Self-Assembled Nickel Hydroxide Three-Dimensional Nanostructures: A Nanomaterial for Alkaline Rechargeable Batteries. *Crystal Growth & Design* **2006,** *7* (1), 170-174.
35. Ida, S.; Shiga, D.; Koinuma, M.; Matsumoto, Y., Synthesis of Hexagonal Nickel Hydroxide Nanosheets by Exfoliation of Layered Nickel Hydroxide Intercalated with Dodecyl Sulfate Ions. *Journal of the American Chemical Society* **2008,** *130* (43), 14038-14039.
36. Arizaga, G. G. C.; Satyanarayana, K. G.; Wypych, F., Layered hydroxide salts: Synthesis, properties and potential applications. *Solid State Ionics* **2007,** *178* (15–18), 1143-1162.
37. Akinc, M.; Jongen, N.; Lemaitre, J.; Hofmann, H., Synthesis of Nickel Hydroxide Powders by Urea Decomposition *Journal of the European Ceramic Society* **1998,** *18* (11), 1559-1564.
38. Soler-Illia, G. J. d. A. A.; Jobbagy, M.; Regazzoni, A. E.; Blesa, M. A., Synthesis of Nickel Hydroxide by Homogeneous Alkalinization. Precipitation Mechanism. *Chemistry of Materials* **1999,** *11*, 3140-3146.
39. M.O. Agwara, P. T. N., M.K. Ndikontar, PHYSICOCHEMECAL STUDIES OF SOME HEXAMETHYLENETETRAMINE
METAL(II) COMPLEXES. *Bull. Chem. Soc. Ethiop.* **2004,** *18(2)*, 143-148.

40. Jiang, H.; Zhao, T.; Li, C.; Ma, J., Hierarchical self-assembly of ultrathin nickel hydroxide nanoflakes for high-performance supercapacitors. *Journal of Materials Chemistry* **2011,** *21* (11), 3818-3823.
41. Jeevanandam, P.; Koltypin, Y.; Gedanken, A., Synthesis of Nanosized α-Nickel Hydroxide by a Sonochemical Method. *Nano Letters* **2001,** *1* (5), 263-266.
42. Cowley, J. M., *Diffraction Physics, Third Edition*. (North-Holland Personal Library), 1995.
43. Brown, T. L., Infrared Spectra of Inorganic and Coordination Compounds. By K. Nakamoto. *Inorganic Chemistry* **1964,** *3* (2), 306-307.
44. Yang, G.-W.; Xu, C.-L.; Li, H.-L., Electrodeposited nickel hydroxide on nickel foam with ultrahigh capacitance. *Chemical Communications* **2008,** (48), 6537-6539.
45. Xu, L.; Ding, Y.-S.; Chen, C.-H.; Zhao, L.; Rimkus, C.; Joesten, R.; Suib, S. L., 3D Flowerlike α-Nickel Hydroxide with Enhanced Electrochemical Activity Synthesized by Microwave-Assisted Hydrothermal Method. *Chemistry of Materials* **2007,** *20* (1), 308-316.
46. Hu, Z.-A.; Xie, Y.-L.; Wang, Y.-X.; Xie, L.-J.; Fu, G.-R.; Jin, X.-Q.; Zhang, Z.-Y.; Yang, Y.-Y.; Wu, H.-Y., Synthesis of α-Cobalt Hydroxides with Different Intercalated Anions and Effects of Intercalated Anions on Their Morphology, Basal Plane Spacing, and Capacitive Property. *The Journal of Physical Chemistry C* **2009,** *113* (28), 12502-12508.
47. Dixit, M.; Subbanna, G. N.; Kamath, P. V., Homogeneous precipitation from solution by urea hydrolysis: a novel chemical route to the [small alpha]-hydroxides of nickel and cobalt. *Journal of Materials Chemistry* **1996,** *6* (8), 1429-1432.
48. Mavis, B.; Akinc, M., Cyanate Intercalation in Nickel Hydroxide. *Chemistry of Materials* **2006,** *18* (22), 5317-5325.
49. Liu, B.-H.; Yu, S.-H.; Chen, S.-F.; Wu, C.-Y., Hexamethylenetetramine Directed Synthesis and Properties of a New Family of α-Nickel Hydroxide Organic−Inorganic Hybrid Materials with High Chemical Stability. *The Journal of Physical Chemistry B* **2006,** *110* (9), 4039-4046.
50. Aghazadeh, M.; Golikand, A. N.; Ghaemi, M., Synthesis, characterization, and electrochemical properties of ultrafine β-Ni(OH)2 nanoparticles. *International Journal of Hydrogen Energy* **2011,** *36* (14), 8674-8679.
51. Ralph H. Petrucci , F. G. H., Jeffry D. Madura General Chemistry: Principles and Modern Applications (10th Edition) Hardcover **May 21, 2010**.
52. Marcus, Y., Ionic radii in aqueous solutions. *Chemical Reviews* **1988,** *88* (8), 1475-1498.
53. Sun, D.; Zhang, J.; Ren, H.; Cui, Z.; Sun, D., Influence of OH− and SO42− Anions on Morphologies of the Nanosized Nickel Hydroxide. *The Journal of Physical Chemistry C* **2010,** *114* (28), 12110-12116.

54. Stranski, I. N.; Klipping, G.; Bogenschuetz, A. F.; Heinrich, H. J.; Maennig, H., 43 Thermal Decomposition of Hexamethylenetetramine. In *Advances in Catalysis*, Adalbert, F., Ed. Academic Press: 1957; Vol. Volume 9, pp 406-414.
55. Cavani, F. T., F.; Vaccari,, Hydrotalcite-type anionic clays: Preparation, properties and applications. *A.Catal. Today* **1991,** *11* (173).
56. Xu, Z. P.; Zeng, H. C., Control of Surface Area and Porosity of Co3O4 via Intercalation of Oxidative or Nonoxidative Anions in Hydrotalcite-like Precursors. *Chemistry of Materials* **2000,** *12* (11), 3459-3465.
57. Jayalakshmi, M.; Radhika, P.; Raja, K. P.; Rao, M. M., Solvent and thiourea adsorption/intercalation effects on the solid-state electrochemistry of α-phase nickel hydroxide nanoparticles. *J Solid State Electrochem* **2007,** *11* (2), 165-172.
58. Ertaş, F. S.; Kaş, R.; Ünal, U.; Birer, Ö., Sonochemical synthesis and electrochemical characterization of α-nickel hydroxide: precursor effects. *J Solid State Electrochem* **2013,** *17* (5), 1455-1462.
59. Xiao, L.; Lu, J.-t.; Liu, P.-f.; Zhuang, L.; Yan, J.; Hu, Y.; Mao, B.; Lin, C., Proton Diffusion Determination and Dual Structure Model for Nickel Hydroxide Based on Potential Step Measurements on Single Spherical Beads. *The Journal of Physical Chemistry B* **2005,** *109* (9), 3860-3867.
60. Zhao, D.-D.; Bao, S.-J.; Zhou, W.-J.; Li, H.-L., Preparation of hexagonal nanoporous nickel hydroxide film and its application for electrochemical capacitor. *Electrochemistry Communications* **2007,** *9* (5), 869-874.
61. Wu, M.-S.; Huang, Y.-A.; Yang, C.-H.; Jow, J.-J., Electrodeposition of nanoporous nickel oxide film for electrochemical capacitors. *International Journal of Hydrogen Energy* **2007,** *32* (17), 4153-4159.
62. Li, H. B.; Yu, M. H.; Wang, F. X.; Liu, P.; Liang, Y.; Xiao, J.; Wang, C. X.; Tong, Y. X.; Yang, G. W., Amorphous nickel hydroxide nanospheres with ultrahigh capacitance and energy density as electrochemical pseudocapacitor materials. *Nat Commun* **2013,** *4*, 1894.
63. Lee, J. W.; Ko, J. M.; Kim, J.-D., Hierarchical Microspheres Based on α-Ni(OH)2 Nanosheets Intercalated with Different Anions: Synthesis, Anion Exchange, and Effect of Intercalated Anions on Electrochemical Capacitance. *Journal of Physical Chemistry C* **2011,** *115*, 19445–19454.

Curriculum Vitae

F. Sinem ERTAŞ was born in Balıkesir (Aegean Region of Turkey) on Februrary 18, 1990. As a undergraduate student she worked at Dr. Funda Yağcı Acar'on Quantum Dot and Polymer Chemistry and Dr. Özgür Birer's Surface Chemistry Group. After finishing her Bachelor in Chemistry at Koç University/ Turkey 2012 she continued to Istanbul to get her Master of Science degree at Koç University after graduation (2012). She got her Master in Material Science and Engineering on September 2014. She published 2 articles in undergraduate semesters and 2 articles in master degree.